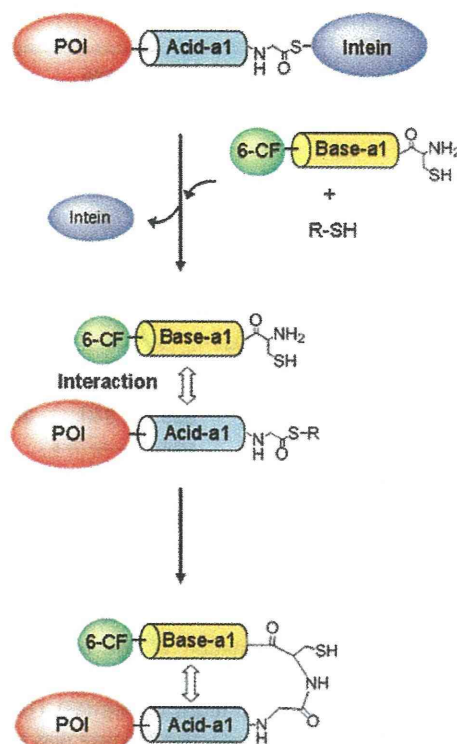


## Noncovalent-Interaction-Promoted Ligation for Protein Labeling

Yuichiro Hori, Yuka Egashira, Ryosuke Kamiura, and Kazuya Kikuchi\*<sup>[a]</sup>

Chemical labeling of proteins with fluorescent probes, isotopes, or other functional compounds provides valuable information that cannot be obtained through conventional biochemistry or molecular biology methods.<sup>[1,2]</sup> In particular, expressed protein ligation (EPL) is a powerful labeling method for analyzing protein function and structure, and has been widely applied to C-terminal labeling of proteins of interest (POI).<sup>[3]</sup> In EPL, proteins with a C-terminal thioester are linked to peptides (or proteins) with an N-terminal Cys by transthioesterification, and an amide bond is subsequently formed. The critical component of this technology is intein,<sup>[4]</sup> which is essential for generating thioester at the protein's C terminus. The major advantage of this technique is that the ligation reaction is considerably chemoselective and, thus, a desirable semisynthetic protein is reliably obtained. However, the reaction is generally inefficient and, therefore, a high concentration (mM or sub-mM) of reactants is required for efficient ligation.<sup>[2,3,5,6]</sup> Consequently, when the solubility of the reactants in water is low, a solubilization reagent, such as guanidine hydrochloride or a surfactant, is used to solubilize the reactants.<sup>[2,6]</sup> This limitation significantly hinders the application of this method to proteins that do not retain their structure and function after removal of the solubilizing reagent. In addition, barring a few exceptions,<sup>[7]</sup> this technique has not been applied to protein labeling in mammalian cell lysate or living cells because the protein expression level is not high enough for the ligation reaction. To overcome these obstacles, we developed a novel protein labeling method based on noncovalent interaction and intein-mediated ligation. This method allows efficient and specific protein labeling in cell lysate by using a low concentration range of thioester protein and synthetic peptide probe.

In order to attain efficient protein labeling, affinity tags were introduced into the reactants. This ensured that the local concentrations of the reactants would increase. As a result, it is expected that the ligation reaction would occur at low concentration. The affinity tags, Acid-a1 and Base-a1,<sup>[8]</sup> which form an antiparallel coiled coil, were chosen because these peptides are small (30 amino acids) and the interaction mechanism is well-known.<sup>[8,9]</sup> In the present research, interaction of the coiled coil was combined with the intein-mediated ligation for protein labeling (Scheme 1). Maltose binding protein (MBP) was employed as a model POI and Acid-a1 was fused to its C terminus (MBP-Acid). The intein was further connected to the C terminus of MBP-Acid to generate a fusion protein MBP-



**Scheme 1.** Principle of protein labeling based on noncovalent coiled-coil interaction and intein-mediated ligation. Coiled coils are represented by Base-a1 and Acid-a1; POI: protein of interest; 6-CF: 6-carboxyfluorescein.

Acid-In, which could form a thioester in the C terminus of MBP-Acid. As a labeling reagent, fluorescein-conjugated Base-a1 (F-Base), which contains Cys at its N terminus, was prepared with Fmoc solid phase method. Acid-a1 with C-terminal thioester (Acid-T) was also synthesized for interaction analysis and model ligation with F-Base.

First, circular dichroism (CD) spectra were measured to determine whether coiled-coil interaction was retained despite the modification of the peptides and the fusion of Acid-a1 with protein domains. Both F-base and Acid-T showed a CD spectrum characteristic of disordered secondary structures (Figure 1A). The addition of F-base to Acid-T resulted in a dramatic increase in negative Cotton effects at 208 and 222 nm. These results indicate that the peptides interact with each other to form  $\alpha$ -helical structures. In contrast with the peptides, the CD spectrum of MBP-Acid-In in the absence of F-Base showed that MBP-Acid-In contains ordered secondary structures, including  $\alpha$ -helices (Figure 1B). This is consistent with previous reports on the crystal structures of those proteins.<sup>[10,11]</sup> The signal of MBP-Acid-In in the far-UV region intensified in the presence of F-Base; this demonstrates that the  $\alpha$ -helix content increased. Thus, these results suggest that F-base

[a] Dr. Y. Hori, Y. Egashira, R. Kamiura, Prof. K. Kikuchi  
Graduate School of Engineering, Osaka University  
2-1 Yamadaoka, Suita, Osaka 565-0871 (Japan)  
Fax: (+81) 6-6879-7875  
E-mail: kkikuchi@mils.eng.osaka-u.ac.jp

Supporting information for this article is available on the WWW under <http://dx.doi.org/10.1002/cbic.201000007>.

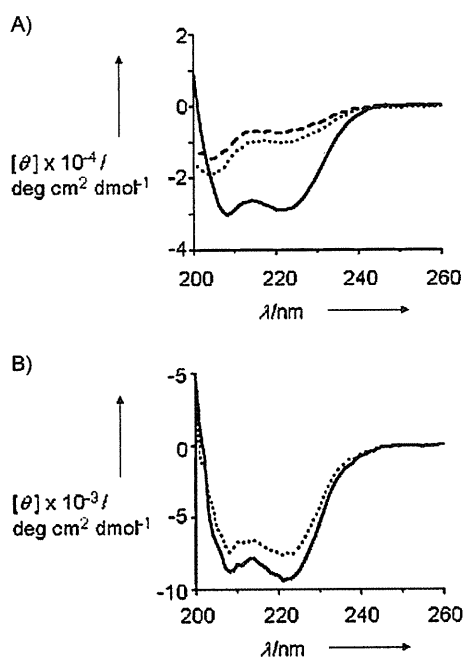


**Figure 1.** CD analyses of structural change in the coiled coils. A) CD spectra of F-Base (-----), Acid-T (.....), and their complex (—). B) CD spectra of MBP-Acid-In in the absence (.....) or presence (—) of F-Base.

binds to the segment of Acid-a1 in MBP-Acid-In and that this association induces the formation of the  $\alpha$ -helix. Next, the model ligation reaction between F-Base and Acid-T was conducted by using low concentrations of peptides (10  $\mu\text{M}$ ). After a 12 h incubation period, the reaction mixture was analyzed by using HPLC (Figure S1 in the Supporting Information). Whereas the retention times of F-Base and Acid-T were 17 and 30 min, respectively, the sample after the reaction eluted at 20 min. ESI-TOF MS showed that the mass value of the eluted fraction was 8051.4, which corresponds to the theoretical mass value of the covalent ligation product (Figure S2 in the Supporting Information). This confirms that the reaction of the synthetic peptides can proceed in this concentration range.

Furthermore, the ligation reaction of F-Base and MBP-Acid-In was carried out in order to examine whether protein labeling occurs at a concentration of 5  $\mu\text{M}$ . MBP-Acid-In was incubated with F-Base at 25 °C for 12 h and the labeling reaction was evaluated with SDS-PAGE. In addition to the band (69 kDa) representing MBP-Acid-In, three other bands appeared at 50, 46, and 23 kDa (Figure 2A). The band at 50 kDa corresponds to the molecular weight of F-base-conjugated MBP-Acid and was fluorescent, while the other two bands at 23 and 46 kDa can be assigned to intein and unligated MBP-Acid cleaved from MBP-Acid-In, respectively. These results indicate that MBP-Acid is labeled with F-base through a covalent bond and that the intein segment is removed as expected. This labeling reaction required MESNA (sodium 2-mercaptoethanesulfonate), which is also necessary in conventional EPL reactions.<sup>[2,3,5]</sup>

To verify the importance of the coiled-coil interaction, we carried out a labeling reaction with MBP-Acid-In and peptide CG3K(6-CF)G, which does not contain Base-a1, but has N-termi-

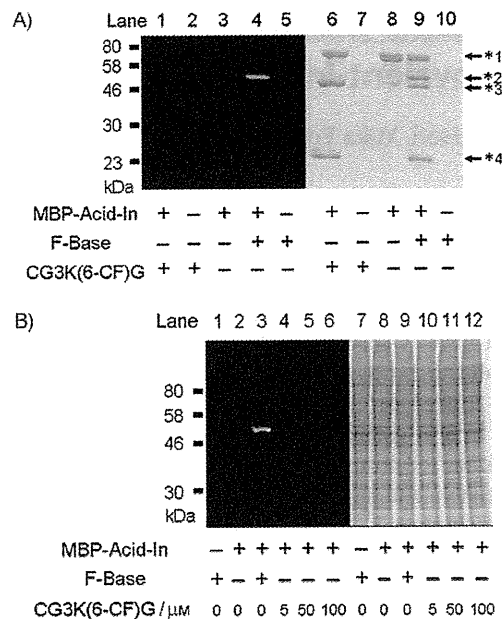


**Figure 2.** SDS-PAGE analyses of protein labeling experiments. Fluorescence and Coomassie Brilliant Blue-stained images are displayed on the left and right, respectively. MESNA (50 mM) was added to reaction mixtures only when they contained both MBP-Acid-In and peptide (F-Base or CG3K(6-CF)G). A) In vitro reactions of MBP-Acid-In (5  $\mu\text{M}$ ) with F-Base (5  $\mu\text{M}$ ) or CG3K(6-CF)G (5  $\mu\text{M}$ ) for 12 h at 25 °C. Asterisks 1–4 designate 69, 50, 46, and 23 kDa bands. B) Labeling reactions of MBP-Acid-In (5  $\mu\text{M}$ ) with F-Base (5  $\mu\text{M}$ ) or CG3K(6-CF)G (5, 50, or 100  $\mu\text{M}$ ) for 12 h at 25 °C in cell lysate.

nal Cys. Figure 2A shows that no fluorescent band derived from CG3K(6-CF)G was produced in lane 1 under these experimental conditions. This result clearly demonstrates that coiled-coil interaction is essential for efficient ligation. The strength of the noncovalent interaction between F-Base and MBP-Acid-In was investigated with fluorescent polarization assay in the absence of MESNA so that no ligation could occur (Figure 3). By conducting titration experiments, the dissociation constant was determined to be  $(7.8 \pm 2.6) \times 10^{-8}$  M. The moderate affinity might not be sufficient for stable protein labeling with only the noncovalent interaction.<sup>[12]</sup> In contrast, in our method, the covalent ligation promoted by noncovalent interaction results in stable protein modification.

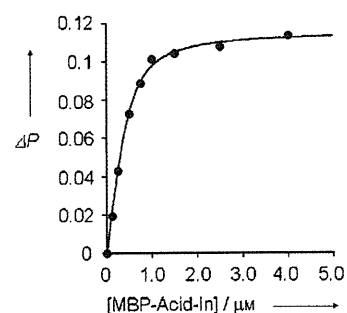


**Figure 3.** Determination of the dissociation constant of F-Base and MBP-Acid-In by a titration experiment. Change in fluorescence polarity ( $\Delta P$ ) of F-Base was plotted against the concentration of MBP-Acid-In.

Finally, in order to clarify the specificity of the labeling, a reaction in cell lysate was performed (Figure 2B). The lysate was prepared from HEK293T cells and added to the reaction mixture. A single fluorescent band was observed in the gel only when F-base was reacted with MBP-Acid-In, demonstrating that the labeling reaction is specific. Moreover, labeling with CG3K(6-CF)G was not detected despite the incubation of the peptide with MBP-Acid-In at a higher peptide concentration (100  $\mu\text{M}$ ). These results indicate that the presence of the coiled-coil interaction contributes significantly to specific protein labeling as well as to the reactivity of the probe.

In conclusion, we constructed a novel system for protein labeling by utilizing a coiled-coil tag and intein. The combination of a noncovalent interaction with a covalent ligation is an effective strategy for efficient and stable modification of proteins. Importantly, the size of the coiled-coil tag is small, and specific labeling is achieved in mammalian cell lysate by using a practical concentration of peptide-based labeling reagent and target protein. These properties are highly attractive for protein detection and visualization in a complex biological environment. Hence, this technique should provide a useful approach in biochemical and biological research.

## Experimental Section

See the Supporting Information for experimental details.

## Acknowledgements

This work was supported by MEXT of Japan (Grants 19021028, 19036012, 20011005, 20675004 to K.K. and 20790099 to Y.H.). We thank Prof. Shigenori Kanaya and Dr. Yuichi Koga at Osaka University for the use of CD spectropolarimeter, Prof. Kazuhiko Nakatani and Dr. Chikara Dohno at Osaka University for the use of MALDI-TOF mass spectrometer, and Prof. Shiroh Futaki and Dr.

Ikuhiko Nakase at Kyoto University and Dr. Tatsuto Kiwada at Kanazawa University for giving advice on peptide synthesis.

**Keywords:** coiled coils · fluorescence · intein-mediated ligation · protein labeling · protein modifications

- [1] a) I. Chen, A. Y. Ting, *Curr. Opin. Biotechnol.* **2005**, *16*, 35–40; b) J. A. Prescher, C. R. Bertozzi, *Nat. Chem. Biol.* **2005**, *1*, 13–21; c) S. S. Gallagher, J. E. Sable, M. P. Sheetz, V. W. Cornish, *ACS Chem. Biol.* **2009**, *4*, 547–556; d) A. Gautier, A. Juillerat, C. Heinis, I. R. Corr ea, Jr., M. Kindermann, F. Beaufils, K. Johnsson, *Chem. Biol.* **2008**, *15*, 128–136; e) M. K. So, H. Yao, J. Rao, *Biochem. Biophys. Res. Commun.* **2008**, *374*, 419–423.
- [2] R. R. Flavell, P. Kothari, M. Bar-Dagan, M. Synan, S. Vallabhajosula, J. M. Friedman, T. W. Muir, G. Ceccarini, *J. Am. Chem. Soc.* **2008**, *130*, 9106–9112.
- [3] a) K. Alexandrov, I. Heinemann, T. Durek, V. Sidorovitch, R. S. Goody, H. Waldmann, *J. Am. Chem. Soc.* **2002**, *124*, 5648–5649; b) J. P. Pellois, M. E. Hahn, T. W. Muir, *J. Am. Chem. Soc.* **2004**, *126*, 7170–7171; c) R. R. Flavell, T. W. Muir, *Acc. Chem. Res.* **2009**, *42*, 107–116; d) D. Schwarzer, P. A. Cole, *Curr. Opin. Chem. Biol.* **2005**, *9*, 561–569.
- [4] T. C. Evans, Jr., M. Q. Xu, *Biopolymers* **1999**, *51*, 333–342.
- [5] a) U. Arnold, M. P. Hinderaker, B. L. Nilsson, B. R. Huck, S. H. Gellman, R. T. Raines, *J. Am. Chem. Soc.* **2002**, *124*, 8522–8523; b) P. S. Hauser, R. O. Ryan, *Protein Expression Purif.* **2007**, *54*, 227–233.
- [6] D. Schwarzer, Z. Zhang, W. Zheng, P. A. Cole, *J. Am. Chem. Soc.* **2006**, *128*, 4192–4193.
- [7] a) R. Y. Lue, G. Y. Chen, Y. Hu, Q. Zhu, S. Q. Yao, *J. Am. Chem. Soc.* **2004**, *126*, 1055–1062; b) L. P. Tan, R. Y. Lue, G. Y. Chen, S. Q. Yao, *Bioorg. Med. Chem. Lett.* **2004**, *14*, 6067–6070.
- [8] M. G. Oakley, P. S. Kim, *Biochemistry* **1998**, *37*, 12603–12610.
- [9] E. K. O'Shea, K. J. Lumb, P. S. Kim, *Curr. Biol.* **1993**, *3*, 658–667.
- [10] F. A. Quioco, J. C. Spurlino, L. E. Rodseth, *Structure* **1997**, *5*, 997–1015.
- [11] T. Klabunde, S. Sharma, A. Telenti, W. R. Jacobs, Jr., J. C. Sacchettini, *Nat. Struct. Biol.* **1998**, *5*, 31–36.
- [12] a) L. W. Miller, Y. Cai, M. P. Sheetz, V. W. Cornish, *Nat. Methods.* **2005**, *2*, 255–257; b) H. E. Rajapakse, D. R. Reddy, S. Mohandessi, N. G. Butlin, L. W. Miller, *Angew. Chem.* **2009**, *121*, 5090–5092; *Angew. Chem. Int. Ed.* **2009**, *48*, 4990–4992.

Received: January 5, 2010

Published online on February 19, 2010

DOI: 10.1002/cbic.200900649

## Application of a Stimuli-Responsive Polymer to the Development of Novel MRI Probes

Satoshi Okada, Shin Mizukami, and Kazuya Kikuchi\*<sup>[a]</sup>

Magnetic resonance imaging is a medical diagnostic tool that is attracting considerable attention as a molecular-imaging technique; this is because MRI is a noninvasive imaging technique that provides information about the internal structure of living organisms. Recently, various chemically modified MRI contrast agents have been developed in order to study in vivo phenomena. These contrast agents, termed "MRI probes", have various functions and include probes that detect enzyme activities, variations in pH, the ionic concentration, and so on.<sup>[1]</sup> In order to change the probes' relaxivities by external stimuli, probes were designed to accommodate a certain number of bound water molecules per gadolinium ion.<sup>[1a]</sup> Other probes involved the attachment of macromolecules, such as proteins, to change the molecular mobility of the probe.<sup>[1b]</sup> However, the rational development of such MRI probes is at an early stage, and the strategies for developing MRI probes are limited.

In order to design novel MRI probes, we focused our attention on stimuli-responsive polymers, which can change their conformation in response to external stimuli such as chemicals, temperature, and pH.<sup>[2]</sup> Stimuli-responsive polymers that exhibit large conformational changes have been developed for applications in drug-delivery systems, functional polymeric matrices, and artificial tissues. To the best of our knowledge, there has been no report regarding the application of stimuli-responsive polymers to the development of MRI probes. In this study, a novel MRI probe was developed by employing a strategy based on conformational changes in stimuli-responsive polymers. We demonstrated that this principle of probe design is useful in detecting pH changes. Additionally, we investigated in detail the stimuli-responsive mechanism of the probe.

pH-responsive polymers were chosen for the development of the probe due to their high potential in clinical applicability for monitoring diseases such as kidney disorder and cancer. The relaxivities of MRI probes are influenced by their rotational motions; therefore, if a pH-responsive conformational change in the probe induces rotational mobility of the Gd<sup>III</sup> complexes attached to the probe, pH variations would lead to alterations in the probe relaxivity. We designed a pH-responsive MRI probe, P-Gd, by attaching clinically used Gd<sup>III</sup> complexes and dansyl chromophores to a pH-responsive polymer, *n*-octylamine-modified poly(sodium maleate-*alt*-ethyl vinyl ether) (poly(SM-EVE); Figure 1). At a low pH, *n*-octylamine-modified poly(SM-EVE) takes on a compact globule conformation because of

the intramolecular hydrophobic interactions among the *n*-octyl groups.<sup>[3]</sup> In contrast, at a high pH, the polymer conformation expands because of the electrostatic repulsion among the deprotonated carboxy groups. Therefore, it is assumed that the molecular rotation of the side chains of the polymer is restricted at low pH, and that the side chains in the expanded conformation rotate more rapidly at a high pH.

In order to elucidate the pH-dependent changes in the polymer shape, we synthesized an aminoethyl-modified Gd(DO3A) complex (Gd(AEDO3A)) and dansyl ethylenediamine, as previously described by Li et al.<sup>[4]</sup> and Shea et al.,<sup>[5]</sup> respectively. Platform polymer poly(SM-EVE) anhydride was synthesized and then modified with *n*-octylamine according to the scheme reported by Hu et al.<sup>[6]</sup> After attaching the Gd<sup>III</sup> complexes and the dansyl chromophores to the *n*-octylamine-modified polymers, the residual carboxylic anhydride groups in the polymer were hydrolyzed with 1 M aqueous NaOH. The polymers were dialyzed and lyophilized to yield P-Gd (Scheme S1 in the Supporting Information). Constituents of octyl groups and Gd<sup>III</sup> were estimated by using elemental analysis and ICP-MS. The approximate molecular weight of the platform polymer was determined by GPC after it was hydrolyzed by the alkaline aqueous solution.

Thereafter, in order to demonstrate the possibility of using P-Gd as a pH-responsive MRI probe, the relaxivities of P-Gd at pH 4–10 were measured. The longitudinal and transverse relaxivities ( $r_1$  and  $r_2$ , respectively) increased as the pH decreased and were maximal at pH 4, while the relaxivities of Gd(AEDO3A) did not increase (Figure 2). This result is consistent with the expected pH-responsive behavior of *n*-octylamine-modified poly(SM-EVE).<sup>[3]</sup> It is assumed that the limited rotational motion of the side chains caused the increase in relaxivities at a low pH. By replacing the carboxy groups of the polymer side chains with functional groups whose  $pK_a$  is near to physiological pH, such as sulfonamide, P-Gd could allow pathological tissues in which the extracellular pH is acidic to be imaged.

The mechanism of variation in relaxation time was investigated as follows. In order to verify the conformational change in P-Gd, its fluorescence spectra were measured. The dansyl group is known to be an environmentally sensitive chromophore. The fluorescence emission spectra of the dansyl group exhibit a blue shift and their intensity increases as the group's surroundings become hydrophobic.<sup>[7]</sup> Therefore, we can obtain information about the conformation of P-Gd from the emission spectra of the dansyl groups attached to the polymer side chains. As the solution pH decreased, the emission spectra of P-Gd exhibited a shift toward shorter wavelengths with an increase in the fluorescence intensity, while the emission spectra of *N*-acetyl-*N'*-dansyl ethylenediamine, which is a monomer

[a] S. Okada, Dr. S. Mizukami, Prof. K. Kikuchi  
Graduate School of Engineering, Osaka University  
2-1 Yamadaoka, Suita City, Osaka 565-0871 (Japan)  
Fax: (+81) 6-6879-7875  
E-mail: kkikuchi@mils.eng.osaka-u.ac.jp

Supporting information for this article is available on the WWW under <http://dx.doi.org/10.1002/cbic.200900775>.



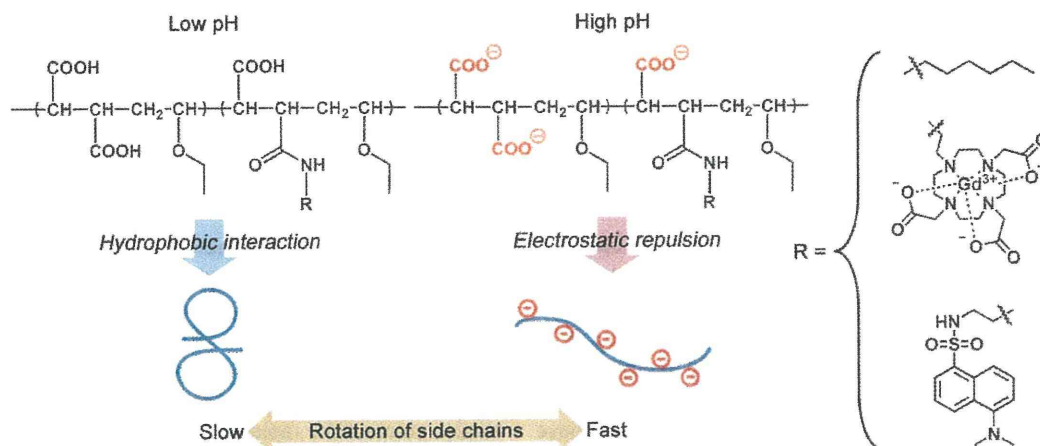


Figure 1. pH-responsive conformational change in the *n*-octylamine-modified poly(SM-EVE)-based MRI probe, P-Gd.

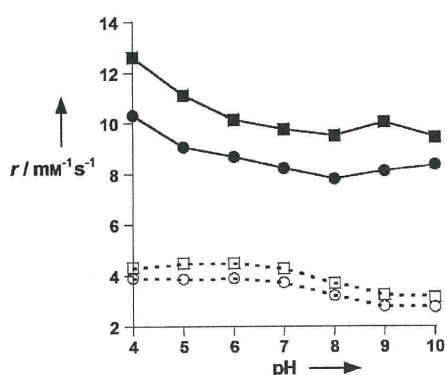


Figure 2. pH profile of the relaxivities of P-Gd (filled symbols) and Gd-(AEDO3A) (open symbols) at 20 MHz and 37 °C. *r* is expressed per Gd<sup>III</sup> ion; circles: *r*<sub>1</sub>, squares: *r*<sub>2</sub>.

model compound of P-Gd, did not shift or increase (Figure 3). These results indicate the build up of a hydrophobic environment around the dansyl groups as the P-Gd conformation becomes globular at a low pH. In contrast, P-Gd expanded in al-

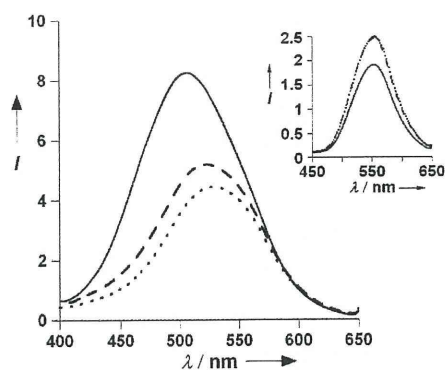


Figure 3. Fluorescence spectra of 0.05% (w/v) P-Gd and 25 μM *N*-acetyl-*N'*-dansyl ethylenediamine in 100 mM phosphate buffer at 37 °C.  $\lambda_{\text{ex}} = 330$  nm; —: pH 4, - - -: pH 6, ···: pH 8. Inset: *N*-acetyl-*N'*-dansyl ethylenediamine.

kaline solution, and the emission spectra indicate the presence of a hydrophilic environment around the dansyl groups. This conformational change is the result of the intramolecular electrostatic repulsion of the carboxylate anions.

In order to reveal the correlation between the probe relaxivity and the polymer mobility, we estimated the rotational correlation times,  $\tau_R$ , of the polymer side chains at different pHs.  $\tau_R$ , which indicates the mobility of the polymer side chains, can be estimated from the values of the fluorescence anisotropy *r* and the fluorescence lifetime  $\tau_F$  of P-Gd by using the Perrin-Weber equation [Eq. (1)].<sup>[8]</sup>

$$r_0/r = 1 + \tau_F/\tau_R \quad (1)$$

Here,  $r_0$  represents the limiting value of *r* in a medium where no rotational diffusion occurs and where the Brownian motion is frozen.  $r_0$  for the dansyl chromophore was experimentally determined to be 0.325.<sup>[9]</sup> After the fluorescence anisotropy and fluorescence lifetime values had been determined (Figures S1 and S3), the rotational correlation times were calculated and plotted against different pH values (Figure 4). The rotational correlation times varied on a nanosecond timescale

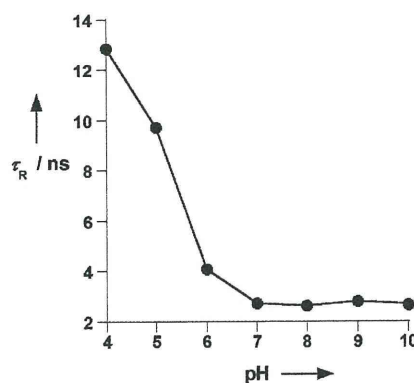


Figure 4. Rotational correlation times of P-Gd in 100 mM phosphate buffer at 25 °C.

and increased at low pH. The pH profile of the rotational correlation time agrees closely with the pH profile of the relaxivity (Figure 2). The rotational correlation times of standard small-molecule contrast agents such as Gd(DOTA)<sup>-</sup> are on the picosecond timescale.<sup>[10]</sup> Because the rotational correlation time of P-Gd is higher than that of the small-molecule contrast agent, the relaxivity of the former is higher than that of the latter.

In conclusion, a novel stimuli-responsive MRI probe has been developed by using a pH-responsive polymer. The relaxivity of the probe was observed to increase with a decrease in the pH of the solution. This pH-responsive mechanism was evaluated in detail through fluorescence studies, which demonstrated that the pH-responsive conformational change caused a change in the rotational correlation time. Thus, we can conclude that relaxivity is pH-dependent. This novel principle of stimuli-responsive polymer conformational change could become a new design strategy for MRI probes or lead to the development of new functional MRI probes.

## Experimental Section

Fluorescence anisotropy  $r$  was measured at pH 4–10 and 25 °C. The fluorescence anisotropy increased as the pH decreased from 7 (Figure S1), thus indicating that, while the rotational motion of the side chains is more pronounced at a high pH, it is restricted at a low pH.

The fluorescence decay curves of P-Gd were acquired in phosphate buffer (100 mM, pH 4–10) at 25 °C (shown in Figure S2 and fitted with double-exponential components; Equation (2)). One of the two components  $\tau_1$  has a long fluorescence lifetime value of ~25 ns, while the other  $\tau_2$  has a short fluorescence lifetime value of ~7 ns. The long-lifetime component increased, its ratio expressed by  $A_1/(A_1+A_2)$ , as the pH decreased. Therefore, the long-lifetime component is consistent with the dansyl groups existing in a hydrophobic environment. In contrast, the short-lifetime component indicates that the dansyl groups were exposed to the aqueous environment.

$$I(t) = A_1 \exp(-t/\tau_1) + A_2 \exp(-t/\tau_2) \quad (2)$$

The weighted-average lifetime was calculated from Equation (3). The fluorescence lifetime grew longer with a decrease in the pH value (Figure S3). This indicates that the environment around the dansyl groups changed due to the conformational change of P-Gd.

$$\tau_f = \tau_1 A_1 / (A_1 + A_2) + \tau_2 A_2 / (A_1 + A_2) \quad (3)$$

## Acknowledgements

We thank Dr. Kei Ohkubo and Prof. Shunichi Fukuzumi at Osaka University for fluorescence lifetime measurements. S.O. expresses his special thanks for the Global COE Program "Global Education and Research Center for Bio-Environmental Chemistry" of Osaka University.

**Keywords:** contrast agents · MRI · polymers · relaxivity · rotational correlation time

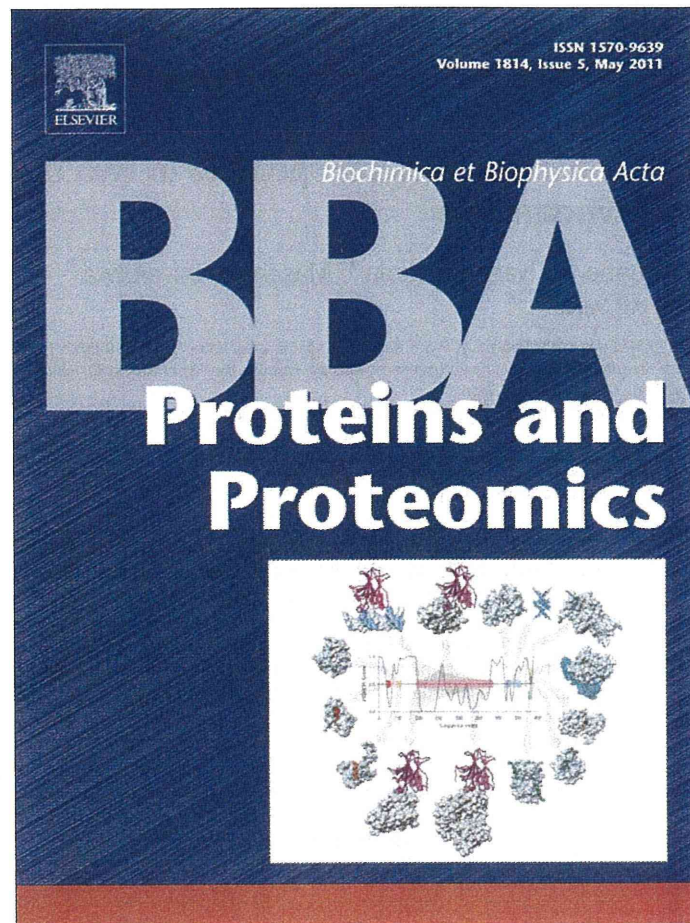
- [1] a) A. Y. Louie, M. M. Hüber, E. T. Ahrens, U. Rothbächer, R. Moats, R. E. Jacobs, S. E. Fraser, T. J. Meade, *Nat. Biotechnol.* **2000**, *18*, 321; b) J. M. Perez, L. Josephson, T. O'Loughlin, D. Högemann, R. Weissleder, *Nat. Biotechnol.* **2002**, *20*, 816; c) W.-h. Li, S. E. Fraser, T. J. Meade, *J. Am. Chem. Soc.* **1999**, *121*, 1413; d) S. Zhang, K. Wu, A. D. Sherry, *Angew. Chem.* **1999**, *111*, 3382; *Angew. Chem. Int. Ed.* **1999**, *38*, 3192; e) S. Aime, A. Barge, D. D. Castelli, F. Fedeli, A. Mortillaro, F. U. Nielsen, E. Terreno, *Magn. Reson. Med.* **2002**, *47*, 639; f) P. Caravan, B. Das, S. Dumas, F. H. Epstein, P. A. Helm, V. Jacques, S. Koerner, A. Kolodziej, L. Shen, W.-C. Sun, Z. Zhang, *Angew. Chem.* **2007**, *119*, 8319; *Angew. Chem. Int. Ed.* **2007**, *46*, 8171; g) G. Liu, Y. Li, M. D. Pagel, *Magn. Reson. Med.* **2007**, *58*, 1249; h) T. Chauvin, P. Durand, M. Bernier, H. Meudal, B.-T. Doan, F. Noury, B. Badet, J.-C. Beloeil, É. Tóth, *Angew. Chem.* **2008**, *120*, 4442; *Angew. Chem. Int. Ed.* **2008**, *47*, 4370; i) K. Hanaoka, K. Kikuchi, T. Terai, T. Komatsu, T. Nagano, *Chem. Eur. J.* **2008**, *14*, 987.
- [2] a) S. Han, M. Hagiwara, T. Ishizone, *Macromolecules* **2003**, *36*, 8312; b) D. Neradovic, C. F. v. Nostrum, W. E. Hennink, *Macromolecules* **2001**, *34*, 7589; c) S. Y. Park, Y. H. Bae, *Macromol. Rapid Commun.* **1999**, *20*, 269; d) L.-C. You, F.-Z. Lu, Z.-C. Li, W. Zhang, F.-M. Li, *Macromolecules* **2003**, *36*, 1; e) T. Miyata, N. Asami, T. Uragami, *Nature* **1999**, *399*, 766.
- [3] Y. Hu, R. S. Armentrout, C. L. McCormick, *Macromolecules* **1997**, *30*, 3538.
- [4] C. Li, Y.-X. Li, G.-L. Law, K. Man, W.-T. Wong, H. Lei, *Bioconjugate Chem.* **2006**, *17*, 571.
- [5] K. J. Shea, G. J. Stoddard, D. M. Shavelle, F. Wakui, R. M. Choate, *Macromolecules* **1990**, *23*, 4497.
- [6] Y. Hu, M. C. Kramer, C. J. Boudreaux, C. L. McCormick, *Macromolecules* **1995**, *28*, 7100.
- [7] Y.-H. Li, L.-M. Chan, L. Tyer, R. T. Moody, C. M. Himel, D. M. Hercules, *J. Am. Chem. Soc.* **1975**, *97*, 3118.
- [8] G. Weber, *Biochem. J.* **1952**, *51*, 145.
- [9] Y. Hu, K. Horie, H. Ushiki, *Macromolecules* **1992**, *25*, 6040.
- [10] C. F. G. C. Geraldes, A. D. Sherry, I. Lázár, A. Miseta, P. Bogner, E. Berenyi, B. Sumegi, G. E. Kiefer, K. McMillan, F. Maton, R. N. Muller, *Magn. Reson. Med.* **1993**, *30*, 696.

Received: October 23, 2009

Revised: February 23, 2010

Published online on March 5, 2010

Provided for non-commercial research and education use.  
Not for reproduction, distribution or commercial use.



This article appeared in a journal published by Elsevier. The attached copy is furnished to the author for internal non-commercial research and education use, including for instruction at the authors institution and sharing with colleagues.

Other uses, including reproduction and distribution, or selling or licensing copies, or posting to personal, institutional or third party websites are prohibited.

In most cases authors are permitted to post their version of the article (e.g. in Word or Tex form) to their personal website or institutional repository. Authors requiring further information regarding Elsevier's archiving and manuscript policies are encouraged to visit:

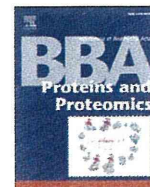
<http://www.elsevier.com/copyright>





Contents lists available at ScienceDirect

## Biochimica et Biophysica Acta

journal homepage: [www.elsevier.com/locate/bbapap](http://www.elsevier.com/locate/bbapap)

## Structural difference of vasoactive intestinal peptide in two distinct membrane-mimicking environments

Yoshitaka Umetsu<sup>a</sup>, Takeshi Tenno<sup>a,b</sup>, Natsuko Goda<sup>a</sup>, Masahiro Shirakawa<sup>b</sup>, Takahisa Ikegami<sup>c</sup>, Hidekazu Hiroaki<sup>a,d,\*</sup><sup>a</sup> Division of Structural Biology, Graduate School of Medicine, Kobe University, 7-5-1 Kusunoki-cho, Chuo-ku, Kobe, Hyogo 650-0017, Japan<sup>b</sup> Department of Molecular Engineering, Graduate School of Engineering, Kyoto University, Katsura, Nishikyo-ku, Kyoto 615-8530, Japan<sup>c</sup> Institute of Protein Research, Osaka University, Suita, Osaka 565-0871, Japan<sup>d</sup> Global Center of Excellence Program for Integrative Membrane Biology, Kobe University, Kobe, Hyogo, Japan

## ARTICLE INFO

## Article history:

Received 14 January 2011

Received in revised form 9 March 2011

Accepted 16 March 2011

Available online 23 March 2011

## Keywords:

Vasoactive intestinal peptide

Pituitary adenylate cyclase-activating peptide

G protein-coupled receptor

NMR structure

Dodecylphosphocholine micelle

## ABSTRACT

Vasoactive intestinal peptide (VIP) is a 28-amino acid neuropeptide which belongs to a glucagon/secretin superfamily, the ligand of class II G protein-coupled receptors. Knowledge for the conformation of VIP bound to membrane is important because the receptor activation is initiated by membrane binding of VIP. We have previously observed that VIP-G (glycine-extended VIP) is unstructured in solution, as evidenced by the limited NMR chemical shift dispersion. In this study, we determined the three-dimensional structures of VIP-G in two distinct membrane-mimicking environments. Although these are basically similar structures composed of a disordered N-terminal region and a long  $\alpha$ -helix, micelle-bound VIP-G has a curved  $\alpha$ -helix. The side chains of residues Phe<sup>6</sup>, Tyr<sup>10</sup>, Leu<sup>13</sup>, and Met<sup>17</sup> found at the concave face form a hydrophobic patch in the micelle-bound state. The structural differences in two distinct membrane-mimicking environments show that the micelle-bound VIP-G localized at the water–micelle boundary with these side chains toward micelle interior. In micelle-bound PACAP-38 (one of the glucagon/secretin superfamily peptide) structure, the identical hydrophobic residues form the micelle-binding interface. This result suggests that these residues play an important role for the membrane binding of VIP and PACAP.

© 2011 Elsevier B.V. All rights reserved.

## 1. Introduction

Vasoactive intestinal peptide (VIP), a member of the glucagon/secretin superfamily, is a 28-amino acid neuropeptide that is evolutionarily well conserved from fish (cod) and frogs to humans. In mammals, except guinea pigs, the sequence identity is at least 85% [1]. VIP widely presents in the central and peripheral nervous systems. It acts in a wide range of physiological and pathological processes related to development, growth, and the control of neuronal and endocrine cells; it also functions in the digestive, respiratory, reproductive, and cardiovascular systems. Furthermore, VIP plays key roles in cancers, immune responses, and circadian rhythm [2]. It is a class II G protein-coupled receptor (GPCR) ligand that acts through interaction with two receptor subtypes (VPAC1 and VPAC2) [3]. VIP shares 68% homology

with its closely related homolog, pituitary adenylate cyclase-activating polypeptide (PACAP), another secretin family member peptide [4,5], and both VIP and PACAP bind to VPAC1 and VPAC2 with equivalent affinities [6]. On binding of VIP to VPAC1 or VPAC2, the cyclic adenosine 5'-phosphate level increases significantly [7], while adenylate cyclase [8] and phospholipase C [9] are also activated, followed by divergent downstream effects through various transcription factors.

Recently, key biological functions of VPAC1 and VPAC2 in innate immune responses have emerged [10], and thus, the therapeutic potential of VIP agonists as well as VIP itself is promising [11]. The increased number of studies supporting the therapeutic potential of VIP includes the murine models of pancreatitis [12], human Crohn's disease (TNBS-induced colitis) [13,14], bacterial sepsis (survival model) [15], and human rheumatoid arthritis (RA; collagen-induced model) [16]. In the first example of the pancreatitis model, a selective VPAC1 agonist rather than VIP itself provides therapeutic benefits because of the opposing action of VPAC2 against VPAC1. In addition, in the other three cases (Crohn's disease, sepsis survival, and RA), the potential anti-inflammatory effect of VIP itself works well, most probably through suppression of inflammatory cytokines such as TNF- $\alpha$  and IL-6.

In addition to the therapeutic use of VIP, specific molecular interactions between VIP–VIP receptors are also useful in diagnosis

**Abbreviations:** NMR, nuclear magnetic resonance; TRX, thioredoxin; PACAP, pituitary adenylate cyclase-activating polypeptide; VIP, vasoactive intestinal peptide; HSQC, heteronuclear single quantum coherence; DPC, dodecylphosphocholine; GPCR, G protein-coupled receptor; RA, rheumatoid arthritis; SAR, structure–activity relationship; TFE, trifluoroethanol

\* Corresponding author at: Division of Structural Biology, Graduate School of Medicine, Kobe University, 7-5-1 Kusunoki-cho, Chuo-ku, Kobe, Hyogo 650-0017, Japan. Tel.: +81 78 382 5813; fax: +81 78 382 5816.

E-mail address: [hiroakih@med.kobe-u.ac.jp](mailto:hiroakih@med.kobe-u.ac.jp) (H. Hiroaki).



of several cancers [17,18]. In cancers such as breast and prostate, an elevated expression of VPAC1 is observed [19]. Thus, accumulation of radio-labeled VIP analogs, such as  $^{99m}\text{Tc}$ -labeled VIP and  $^{64}\text{Cu}$ -labeled TP3939, enables visualization of cancers by positron emission tomography. VPAC receptors temporarily downregulate by endocytosis when VIP binds to them [20]. This mechanism has encouraged researchers to develop VIP analogs as imaging agents.

The 3D structure of VIP and its stability highlight the possible development of drug delivery systems with an improved therapeutic potency of VIP and its analogs. Several VIP formulations with increased biochemical and physicochemical stability have been studied extensively [21–23]. A typical variation for therapeutic VIPs is their incorporation into phospholipids or liposomes. Such variations generally double the activity of VIP. The primary benefit of the lipid/liposome formulation is to protect VIP from enzymatic degradation *in vivo*. In addition, a structural transition from a random coil to an  $\alpha$ -helix on lipid and/or liposome binding is the rate-limiting step at the ligation of VIP to the receptors. A number of structural studies have shown that PACAP [24,25] as well as other class II GPCR ligands [26–29] adopt  $\alpha$ -helical conformations when they bind to the receptor. A pre-existing  $\alpha$ -helical conformation is also important in increasing the biological activities of the peptides [30], which is partly explained by a two-step model demonstrating the PACAP–PAC1R interaction [24]. Thus, the solution structure of VIP in the absence of its receptors and presence of phospholipids is another important issue.

In this study, we focused on the structural analysis of VIP in order to enable us to develop potent VIP analogs using a structure–activity relationship (SAR) study. Previously, the solution structure of VIP in 30% trifluoroethanol (TFE) solution was determined by the  $^1\text{H}$  nuclear magnetic resonance (NMR) technique but not using isotopically labeled peptide [31], thereby showing limited structural convergence. In addition, the structural coordinates were not commonly available, thus limiting SAR studies by other groups. Here we determined the solution structures of VIP-G (28-residue VIP with extra C-terminal glycine, an equivalent peptide of the biosynthetic precursor of VIP before C-terminal amidation) in two different conditions, 50% MeOH, and aqueous buffer containing dodecylphosphocholine (DPC) micelles. Use of isotopically labeled VIP enabled analysis of the NMR spectra in the presence of a large number of DPC micelles in solution. Here we discuss the differences between the two structures in detail.

## 2. Materials and methods

### 2.1. Preparation of $^{15}\text{N}$ - and $^{13}\text{C}/^{15}\text{N}$ -labeled VIP-G

The bacterial expression system with VIP-G as the fusion protein of thioredoxin, followed by a 6-poly histidine tag, factor Xa cleavage site, and VIP-G [thioredoxin (TRX)\_VIP-G], was as described previously [32]. For  $^{15}\text{N}$  and  $^{13}\text{C}/^{15}\text{N}$  labeling of the fusion protein TRX\_VIP-G, M9 medium containing 0.5 g/L  $^{15}\text{N}$ - $\text{NH}_4\text{Cl}$  as the sole nitrogen source and 4 g/L of  $^{12}\text{C}$ -glucose or 2 g/L of  $^{13}\text{C}_6$ -glucose, respectively, were used. *Escherichia coli* BL21(DE3) harboring pET-TRX\_VIP-G was grown in 100 mL of M9 medium containing 50  $\mu\text{g}/\text{mL}$  ampicillin for 16 h. The cells were transferred into 0.9 L cultures of the same medium in 5-L baffled flasks. Isopropyl-D-thiogalactopyranoside induction was performed as described earlier, except that the cells were incubated for 6 h at 30 °C prior to harvesting.

BL21(DE3) cells from 1 L of M9 medium were pelleted, resuspended in 30 mL of 50 mM Tris-HCl (pH 7.5), 0.15 M NaCl, and 10 mM mercaptoethanol, and disrupted by sonication. Cell debris were removed by centrifugation, and the extracts were then passed through a 4-mL column of DEAE-Sepharose. The extracts, cleared by either osmotic disruption or sonication, were loaded onto a 4-mL column of fast-flow chelating Sepharose, previously charged with 50 mM  $\text{NiSO}_4$ , and equilibrated in 20 mM imidazole and 50 mM Tris-HCl (pH 7.5). The column was then washed with 50 mM imidazole and 50 mM Tris-HCl

(pH 7.5), followed by fusion protein elution with 0.2 M of imidazole and 50 mM Tris-HCl (pH 7.5). Fusion proteins eluted from the column (2 mL) were dialyzed against 1 L buffer containing 0.5 M NaCl and 50 mM Tris-HCl (pH 7.5) at 4 °C for 16 h.

### 2.2. NMR spectroscopy

NMR experiments were performed on a Bruker AvanceDRX (500 MHz) or an Bruker Avance III (600 MHz) NMR spectrometer, the latter being equipped with a cryogenic triple-resonance probe. To determine the structure in MeOH, ~400  $\mu\text{g}$  of  $^{13}\text{C}/^{15}\text{N}$ -VIP-G was dissolved in 0.25 mL of 50%–50%  $\text{H}_2\text{O}$ - $\text{d}_3$ -MeOH containing 20 mM Tris-HCl (pH 7.4). For structural determination in a DPC micelle, ~500  $\mu\text{g}$  of  $^{15}\text{N}$ - or  $^{13}\text{C}/^{15}\text{N}$ -VIP-G was dissolved in 0.25 mL of 90%–10%  $\text{H}_2\text{O}$ - $\text{D}_2\text{O}$  containing 50 mM potassium phosphate buffer at pH 7.2, with and without 50 mM DPC micelle. Sodium 2,2-dimethyl-2-silapentane-5-sulfonate was used as a reference for the chemical shift. Heteronuclear single quantum coherence (HSQC) spectra [33] adapted with a gradient sensitivity enhancement [34] were acquired with eight transients and 256 increments at 288 or 298 K, and zero filling during spectral processing. All NMR spectra were recorded at 288 (in MeOH) or 298 K (in DPC micelle). All spectra were processed using NMRPipe [35] and analyzed using the program nmrDraw [35]. Interproton distances were obtained from 3D  $^{13}\text{C}$ - and  $^{15}\text{N}$ -edited HSQC NOESY spectra recorded with a 200-ms (in MeOH) and 150-ms (in DPC micelle) mixing time. Structures were calculated using a standard seven iteration cycle protocol of the program CYANA version 2.0.17 [36,37]. All NOE cross-peaks were selected manually using SPARKY [38]. Dihedral angle restraints were calculated using the TALOS program based on backbone atom chemical shifts [39]. The structural coordinates were deposited to PDB (PDB ID: 2RRH for the structure in MeOH), (PDB ID: 2RRI for the micelle-bound VIP), and the assignments were deposited to BMRB (accession numbers = 11419 and 11420, respectively).

## 3. Results and discussion

### 3.1. Structure of VIP-G in 50% MeOH

Organic solvents such as MeOH or TFE have been used in conformational studies of VIP and its derivatives by CD and/or NMR analysis to determine their SARs. These solvents, either neat or mixed with water, mimic hydrophobic environments, such as the cell membrane or N-terminal ectodomain (N-ted) of VIP receptors. Wild-type VIP is a 28-amino acid peptide having a C-terminal amide moiety. However, Fahrenkrug and co-workers clearly showed that the amide group of the C-terminus of VIP was not very effective for receptor binding or activation [40]. Therefore, glycine-extended VIP (VIP-G) (Fig. 1A) was used for the NMR analysis in this study. We employed  $^{13}\text{C}/^{15}\text{N}$  isotopically labeled VIP-G produced by *E. coli*.

Assignments for the backbone HN, N, C $\alpha$ , C $\beta$ , and C $\gamma$  resonances of VIP-G in 50% MeOH were achieved by analysis of the triple-resonance HNCACB, CBCA(CO)NH, and HNCO spectra according to the standard method [41]. H $\alpha$ , the side-chain proton, and carbon resonances were assigned from the HCC(CO)NH and CC(CO)NH spectra. Fig. 1B shows the assigned  $^1\text{H}$ - $^{15}\text{N}$  HSQC spectra of VIP-G in 50% MeOH. All backbone resonances, except for His<sup>1</sup> and Ser<sup>2</sup>, and 93% of the nonexchangeable protons of the side-chain signals were assigned. Backbone dihedral angle restraints were determined using the TALOS program [39]. TALOS showed an  $\alpha$ -helix in VIP-G between Ala<sup>4</sup> and Ser<sup>25</sup> in 50% MeOH.

The final ensemble of 20 low-energy structures of VIP-G in 50% MeOH was generated from a total of 395 experimental constraints derived by NMR. Many medium-range NOEs showing helix,  $d_{\alpha\text{N}}(i, i+3)$ ,  $d_{\alpha\text{P}}(i, i+3)$ , and  $d_{\alpha\text{N}}(i, i+4)$  were observed among residues Val<sup>5</sup>–Gly<sup>29</sup> (Supplementary Fig. 1A). The RMSD values of the backbone atoms evaluated for Ala<sup>4</sup>–Asn<sup>28</sup> of the 20 structures were 0.35 Å for the



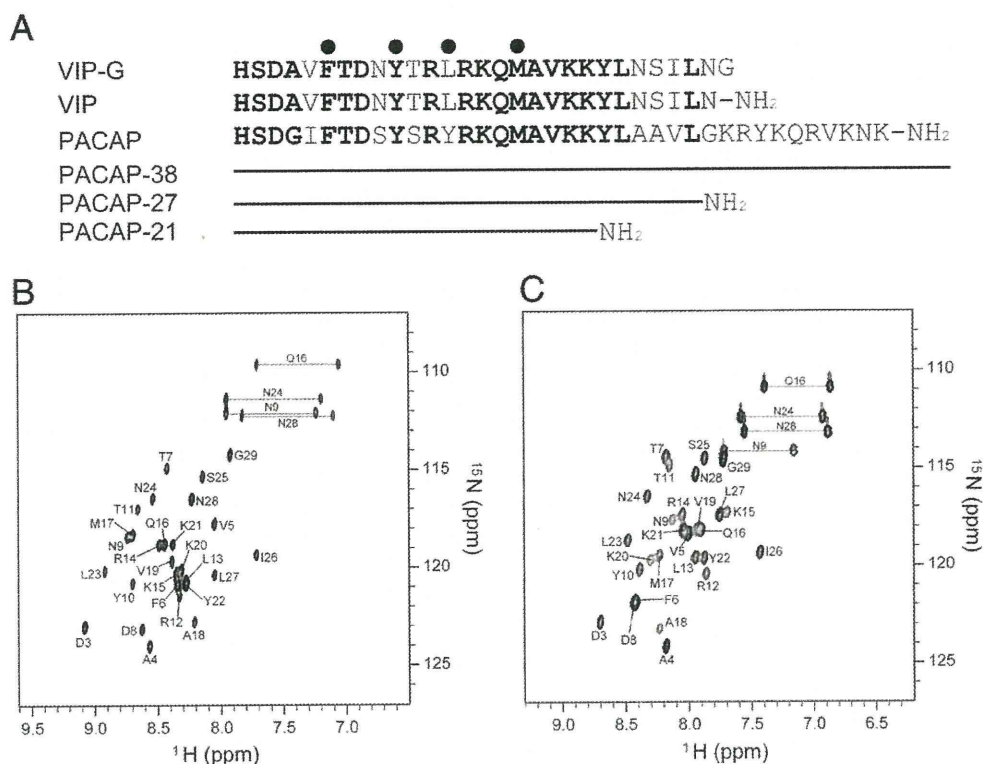


**Fig. 1.** Amino acid sequence and  $^1\text{H}$ - $^{15}\text{N}$  HSQC spectra. (A) Amino acid sequence of VIP and PACAP. Conserved residues are shown in bold. The filled circles indicate the residues forming a hydrophobic surface facing to DPC micelle. (B) and (C)  $^1\text{H}$ - $^{15}\text{N}$  HSQC spectra in 50% MeOH containing 20 mM Tris-HCl (pH 4.4) at 288 K (B) and in the presence of the 50 mM DPC micelle containing 50 mM potassium phosphate buffer (pH 7.2) at 298 K (C). Spectral cross-peaks are labeled by a 1-letter amino acid code and residue number.

backbone atoms and 0.95 Å for all the heavy atoms. The Ramachandran plot for all refined 20 structures for VIP-G shows that the backbone dihedral angles occupy the most favored or additionally allowed regions (Table 1). Superposition of the backbones of the 20 lowest target function structures in 50% MeOH is shown in Fig. 2. The structure of VIP-G in MeOH contains a central  $\alpha$ -helix region comprising residues 4–29 and unstructured N-terminal regions (residues 1–3) (Fig. 2B).

Tan et al. previously reported the structure of VIP in 30% TFE [31]. The  $\alpha$ -helical contents in 50% MeOH are similar to that in 30% TFE, which is also consistent with CD data. In contrast, the side-chain

conformation is different in 50% MeOH and 30% TFE. In 30% TFE, several side-chain-side-chain interactions have been reported (Asn<sup>9</sup>-Arg<sup>12</sup>, Leu<sup>13</sup>-Met<sup>17</sup>, Val<sup>19</sup>-Leu<sup>23</sup>, and Lys<sup>20</sup>-Asn<sup>24</sup>). However, there were no side-chain interactions in this experiment, although the side-chain structure is well converged (RMSD values < 1.0 Å).

### 3.2. Structure of VIP-G bound to DPC micelle

We then determined the solution structure of VIP-G in the presence of the 50 mM DPC micelle (peptide/DPC ratio, 1:84). DPC is a well-known membrane-mimicking compound and is often used in solution NMR studies of peptide-membrane interactions. A DPC micelle is composed of ~60 DPC molecules in water. DPC has a neutral head group and mimics the nonisotropic environment of a lipid membrane. DPC forms stable micelles, resulting in reasonable correlation time and manageable line width for solution NMR studies. A remarkable difference in the DPC micelle compared with planar lipid bilayers is that the micelles possess a highly curved surface.

The  $^1\text{H}$ - $^{15}\text{N}$  HSQC spectra of VIP-G in the presence of DPC micelles are shown in Fig. 1C. We observed broader cross-peaks on the association of VIP-G to the DPC micelles (molecular mass of the DPC micelle is approximately 20 kDa). When more DPC was added to this sample (peptide/micelle ratio, 1:3), NMR signals were unchanged. Therefore, these NMR signals were from only the bound form within this experimental condition. We assigned all backbone resonances, except for His<sup>1</sup> and Ser<sup>2</sup>, and 93% of the nonexchangeable protons of the side-chain signals. An ensemble of 20 structures with low CYANA target functions was constructed from 376 experimental NMR constraints. The RMSD values after superimposing backbone atoms of Phe<sup>6</sup>-Ile<sup>26</sup> were 0.55 Å and 0.93 Å for backbone and heavy atoms, respectively. The secondary structure of the micelle-bound VIP-G consisted of an  $\alpha$ -helix around Phe<sup>6</sup>-Ile<sup>26</sup> (Fig. 3). The N-terminal

**Table 1**  
Structural statistics for the final 20 structures of VIP in DPC and 50% MeOH.

	MeOH	DPC
Distance restraints		
Total number of NOE restraints	395	376
Intraresidue	Unused	Unused
Sequential restraints ( $ i-j =1$ )	246	246
Medium-range restraints ( $1 <  i-j  \leq 4$ )	149	129
Long-range restraints ( $ i-j  > 5$ )	0	1
Dihedral angle restraints		
$\phi/\psi/\chi$	23/23/0	22/22/0
Hydrogen bond restraints	0	0
Final statistics		
Maximum target function	0.05	0.47
RMSD for experimental structure (Å)		
All backbone atoms (4–28 in MeOH, 6–26 in DPC)	0.35	0.55
All heavy atoms (4–28 in MeOH, 6–26 in DPC)	0.93	0.93
Ramachandran plot statistics (%)		
Most favored region	97.0	89.1
Additionally allowed region	3.0	10.9
Generously allowed region	0.0	0.0
Disallowed region	0.0	0.0

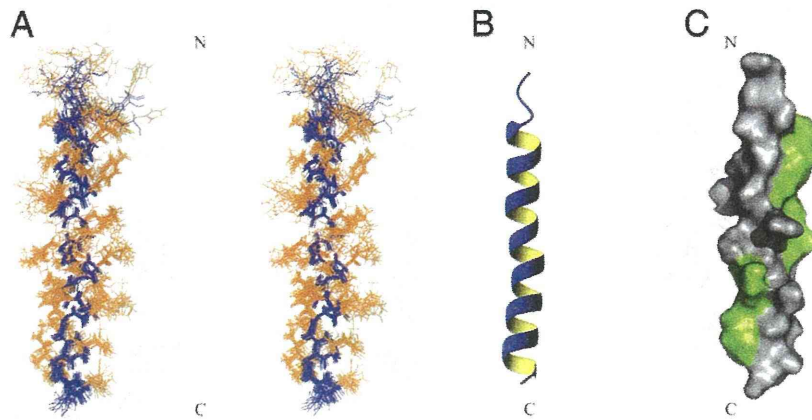


**Fig. 2.** Three-dimensional structures of VIP-G in 50% MeOH. (A) Ensemble of the 20 lowest energy structures of VIP-G in 50% MeOH. The backbone atoms of residues 4–28 were used for the superimposition. (B) and (C) Side views of the ribbon diagram (B) and surface model (C) of VIP-G of a representative conformer. The hydrophobic residues (V, I, L, Y, F, M) are colored green.

region (residues 1–5) was largely disordered, whereas the C-terminal region was more restricted and was close to an  $\alpha$ -helical structure.

### 3.3. Comparison of 50% MeOH- and DPC micelle-bound forms of the VIP-G structure

To determine the interaction at the peptide–membrane interface, we first compared the chemical shift of VIP-G in DPC micelle to that in MeOH. Although the chemical shifts of several peaks were different in DPC and in MeOH, we could not determine the interaction at the VIP-G–micelle interface specifically from the chemical shift data. However, we determined the 3D structure of VIP-G in two different membrane-mimicking environments allowing us to compare two structures. Mapping of the hydrophobic residues on the molecular surface of VIP-G reveals that two hydrophobic patches are located at the opposite side of molecule (Figs. 2C and 3C). Compared with the structure of VIP-G in 50% MeOH, the  $\alpha$ -helix of the micelle-bound form displayed a slight curvature (Fig. 4A and B). The diameter of this curvature was  $21.84 \pm 2.01$  Å, which is similar to the reported size of a DPC micelle (Supplementary Fig. 2) [42]. The side chains of residues Phe<sup>6</sup>, Tyr<sup>10</sup>, Leu<sup>13</sup>, and Met<sup>17</sup> found at the concave face formed a hydrophobic patch in the micelle-bound state. VIP-G localized at the water–micelle boundary with these side chains toward the micelle

interior. Thus, we inferred that this structural difference between the MeOH form and the micelle-bound form was caused by the peptide–micelle interaction on the curved micelle surfaces. Note that these two hydrophobic clusters were largely conserved within VIP and PACAP, which suggests the biological importance of the residues. The hydrophobic cluster consists of Ala<sup>18</sup>, Val<sup>19</sup>, Tyr<sup>22</sup>, Leu<sup>23</sup>, Ile<sup>26</sup>, and Leu<sup>27</sup> located at the peptide–N-terminus interface on the structure of PACAP–PAC1R complex [25]. It is partly consistent with an extensive SAR study on VIP, in which Ala-substituted mutants for each residue were examined [43]. Of course, direct proof of the peptide–lipid interaction of these residues requires further investigation by NMR experiments using spin-labeled DPC analogs.

### 3.4. Comparison of the structure of VIP-G and PACAP

The micelle- and receptor-bound structure of PACAP, which has high sequence homology with VIP, has been reported previously [24]. In this section, we compare our MeOH and micelle-bound forms of the VIP structure with other reported structures. Inooka et al. published a preliminary analysis of the micelle-bound structure of PACAP27, which adopts an  $\alpha$ -helix (data not deposited on PDB). In addition, the micelle-bound structure of PACAP38 (PDB ID 2D2P), which comprises the flexible N-terminus (residues 1–4) followed by the

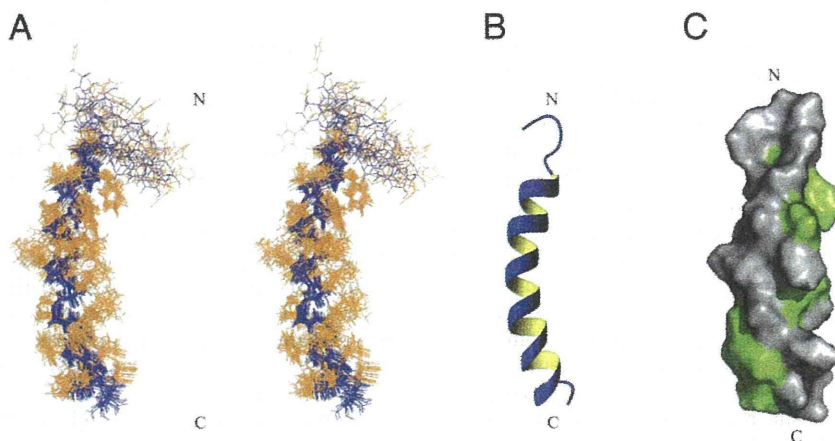


**Fig. 3.** Three-dimensional structures of VIP-G bound to a DPC micelle. (A) Ensemble of the 20 lowest energy structures of VIP-G in the DPC micelle. The backbone atoms of residues 6–26 were used for the superimposition. (B) and (C) Side views of the ribbon diagram (B) and surface model (C) of micelle-bound VIP-G of a representative conformer. The hydrophobic residues (V, I, L, Y, F, M) are colored green.



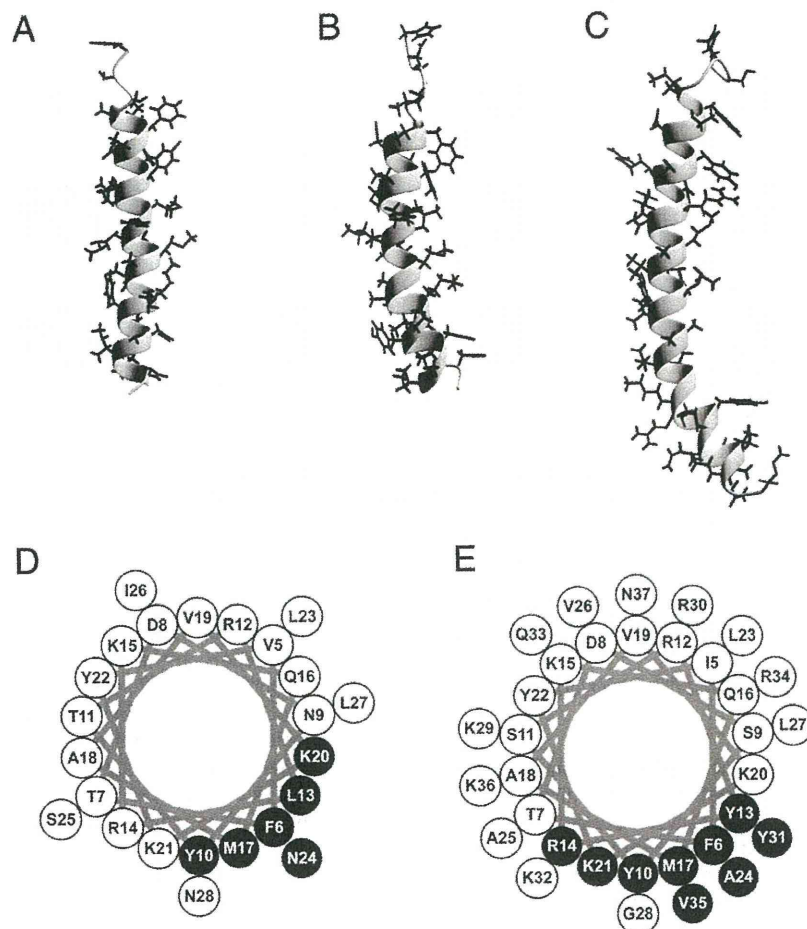


**Fig. 4.** Comparison of the structure of VIP-G and PACAP-38. (A–C) Side views of the ribbon diagram of VIP-G (in MeOH (A) and in the DPC micelle (B)) and PACAP-38 bound to the DPC micelle (C). (D and E) A helical wheel projections of the membrane-bound states of VIP (D) and PACAP (E). Amino acid residues located the peptide–membrane interface are shown in black.

stable  $\alpha$ -helical region (5–38), is substantially similar to that of VIP-G (Fig. 4B and C). In particular, the C-terminal region of PACAP38 adopts a curved helix, which may reflect the curvature of the micelle. Moreover, the identical hydrophobic side chains (Phe<sup>6</sup>, Tyr<sup>10</sup>, Leu<sup>13</sup>, and Met<sup>17</sup>) form a micelle-binding interface inserted into the hydrophobic interior of the DPC micelle (Fig. 4D and E). This result indicates that VIP-G and PACAP have the same micelle-anchoring topology.

The conformations of VIP and PACAP in the lipid bilayer have also been studied, providing a better model for mimicking a cell membrane. A dimyristoylphosphatidylcholine/dimyristoylphosphatidylglycerol-based lipid bilayer was used as the peptide carrier to determine the structure of PACAP21 and PACAP27 using solid state NMR [44]. Interestingly, PACAP21 and PACAP27 adopted extended structures in the lipid bilayer-bound state. Gololobov et al. studied the conformation of VIP in liposomes using CD spectra and showed that VIP forms an  $\alpha$ -helix in the presence of anionic phospholipid phosphatidylglycerol, whereas VIP remains unstructured in the presence of the neutral phospholipid phosphatidylcholine [30]. Although class II GPCR ligands usually adopt  $\alpha$ -helices in the membrane-mimicking environment, VIP and PACAP vary their conformation depending on the environment, which might be unique. Considering the stable  $\alpha$ -helical formation with an anionic lipid bilayer, some conserved cationic residues (Arg<sup>14</sup>, Lys<sup>20</sup>, and Lys<sup>21</sup>) located near the peptide–micelle interface may play an important part in the conformational transition and  $\alpha$ -helical stabilization.

### 3.5. Two-step ligand transportation mechanism of VIP in GPCR activation

As mentioned previously, the biological action of class II GPCR ligands is because of the ligation of peptides to the N-terminus of the receptors. All the examples showed that these ligand peptides adopt an  $\alpha$ -helical conformation on binding to the N-terminus. A two-step ligand transportation model of GPCR activation was suggested [24,45]. Their model proposed that membrane interaction is an important event preceding receptor binding (Fig. 5). Peptide–membrane interaction induces an  $\alpha$ -helical conformation closely homologous to the active one, leading to reduced losses in entropy upon receptor binding.

SAR was investigated by analyzing the biological activities of several variants of VIP. In particular, alanine-scanning studies revealed the key residues for VIP receptor binding or activation [43,46–48]. Modeling of the VIP structure in membrane-mimicking environments or with the receptor was also challenged [31,49]. Unfortunately, the interpretations of the existing pharmacological studies seemed to be controversial and did not succeed in perfectly explaining the mode of VIP action. Therefore, more structural information on VIP is required. In this study, we determined the micelle-bound VIP structure and found that four residues form a hydrophobic interface with the DPC micelle. Mutation on some of these residues showed substantial reduction in the activity of VIP, probably because they destabilized the  $\alpha$ -helix. Thus, the residues in the peptide–membrane interface and those in the peptide–receptor interface must be separately considered in a SAR study.



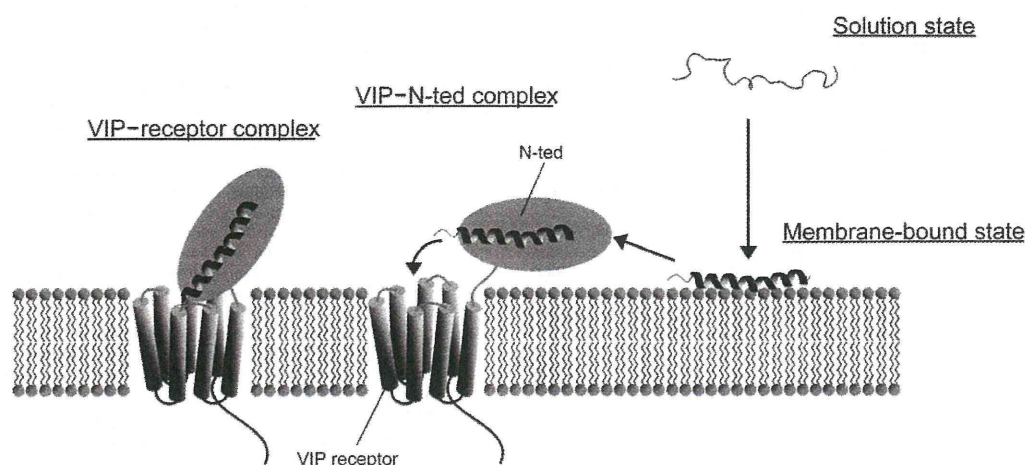


**Fig. 5.** Schematic diagram of the two-step ligand transportation model for VIP. The peptide nonspecifically binds to cell membranes and forms an  $\alpha$ -helix at the C-terminal region. Then, VIP undergoes 2D diffusion to the receptor and binds to the N-ted of the VIP receptor. Finally, VIP is sandwiched between the N-ted and core of the receptor.

In conclusion, we have determined the solution structure of VIP in two distinct membrane-mimicking environments, both of which induced an  $\alpha$ -helix in VIP. The data presented here will provide a rational basis for the development of VIP analogs, which will be useful in therapy for inflammatory diseases as well as cancer diagnoses.

Supplementary materials related to this article can be found online at doi:10.1016/j.bbapap.2011.03.009.

## References

- [1] B.H. Du, J. Eng, J.D. Hulmes, M. Chang, Y.C. Pan, R.S. Yalow, Guinea pig has a unique mammalian VIP, *Biochem. Biophys. Res. Commun.* 128 (1985) 1093–1098.
- [2] S. Onoue, S. Misaka, S. Yamada, Structure–activity relationship of vasoactive intestinal peptide (VIP): potent agonists and potential clinical applications, *Naunyn-Schmiedeberg's Arch. Pharmacol.* 377 (2008) 579–590.
- [3] M. Laburthe, A. Couvineau, V. Tan, Class II G protein-coupled receptors for VIP and PACAP: structure, models of activation and pharmacology, *Peptides* 28 (2007) 1631–1639.
- [4] R.M. Campbell, C.G. Scanes, Evolution of the growth hormone-releasing factor (GRF) family of peptides, *Growth Regul.* 2 (1992) 175–191.
- [5] G.V. Segre, S.R. Goldring, Receptors for secretin, calcitonin, parathyroid hormone (PTH)/PTH-related peptide, vasoactive intestinal peptide, glucagon-like peptide 1, growth hormone-releasing hormone, and glucagon belong to a newly discovered G-protein-linked receptor family, *Trends Endocrinol. Metab.* 4 (1993) 309–314.
- [6] S.R. Rawlings, M. Hezareh, Pituitary adenylate cyclase-activating polypeptide (PACAP) and PACAP/vasoactive intestinal polypeptide receptors: actions on the anterior pituitary gland, *Endocr. Rev.* 17 (1996) 4–29.
- [7] M. Laburthe, M. Rousset, C. Boissard, G. Chevalier, A. Zweibaum, G. Rosselin, Vasoactive intestinal peptide: a potent stimulator of adenosine 3':5'-cyclic monophosphate accumulation in gut carcinoma cell lines in culture, *Proc. Natl. Acad. Sci. U.S.A.* 75 (1978) 2772–2775.
- [8] R. Salomon, A. Couvineau, C. Rouyer-Fessard, T. Voisin, D. Lavallee, A. Blais, D. Darmoul, M. Laburthe, Characterization of a common VIP-PACAP receptor in human small intestinal epithelium, *Am. J. Physiol.* 264 (1993) 294–300.
- [9] C.J. Mackenzie, E.M. Lutz, D.A. McCulloch, R. Mitchell, A.J. Harmar, Phospholipase C activation by VIP1 and VIP2 receptors expressed in COS 7 cells involves a pertussis toxin-sensitive mechanism, *Ann. NY Acad. Sci.* 805 (1996) 579–584.
- [10] D.L. Bellinger, D. Lorton, S. Broukhon, S. Felten, D.L. Felten, The significance of vasoactive intestinal polypeptide (VIP) in immunomodulation, *Adv. Neuroimmunol.* 6 (1996) 5–27.
- [11] S.G. Smalley, P.A. Barrow, N. Foster, Immunomodulation of innate immune responses by vasoactive intestinal peptide (VIP): its therapeutic potential in inflammatory disease, *Clin. Exp. Immunol.* 157 (2009) 225–234.
- [12] M. Kojima, T. Ito, T. Oono, T. Hisano, H. Igarashi, Y. Arita, K. Kawabe, D.H. Coy, R.T. Jensen, H. Nawata, VIP attenuation of the severity of experimental pancreatitis is due to VPAC1 receptor-mediated inhibition of cytokine production, *Pancreas* 30 (2005) 62–70.
- [13] A. Arranz, C. Abad, Y. Juarranz, J. Leceta, C. Martinez, R.P. Gomariz, Vasoactive intestinal peptide as a healing mediator in Crohn's disease, *Neuroimmunomodulation* 15 (2008) 46–53.
- [14] E. Gonzalez-Rey, M. Delgado, Therapeutic treatment of experimental colitis with regulatory dendritic cells generated with vasoactive intestinal peptide, *Gastroenterology* 131 (2006) 1799–1811.
- [15] M. Delgado, C. Martinez, D. Pozo, J.R. Calvo, J. Leceta, D. Ganea, R.P. Gomariz, Vasoactive intestinal peptide (VIP) and pituitary adenylate cyclase-activation polypeptide (PACAP) protect mice from lethal endotoxemia through the inhibition of TNF-alpha and IL-6, *J. Immunol.* 162 (1999) 1200–1205.
- [16] M. Delgado, C. Abad, C. Martinez, J. Leceta, R.P. Gomariz, Vasoactive intestinal peptide prevents experimental arthritis by downregulating both autoimmune and inflammatory components of the disease, *Nat. Med.* 7 (2001) 563–568.
- [17] M.L. Thakur, C.S. Marcus, S. Saeed, V. Pallela, C. Minami, L. Diggles, H. Le Pham, R. Ahdoot, E.A. Kalinowski, 99mTc-labeled vasoactive intestinal peptide analog for rapid localization of tumors in humans, *J. Nucl. Med.* 41 (2000) 107–110.
- [18] M.L. Thakur, M.R. Aruva, J. Gariepy, P. Acton, S. Rattan, S. Prasad, E. Wickstrom, A. Alavi, PET imaging of oncogene overexpression using 64Cu-vasoactive intestinal peptide (VIP) analog: comparison with 99mTc-VIP analog, *J. Nucl. Med.* 45 (2004) 1381–1389.
- [19] J.C. Reubi, In vitro identification of vasoactive intestinal peptide receptors in human tumors: implications for tumor imaging, *J. Nucl. Med.* 36 (1995) 1846–1853.
- [20] C. Boissard, J.C. Marie, G. Hejblum, C. Gespach, G. Rosselin, Vasoactive intestinal peptide receptor regulation and reversible desensitization in human colonic carcinoma cells in culture, *Cancer Res.* 46 (1986) 4406–4413.
- [21] I. Rubinstein, Human VIP-alpha: an emerging biologic response modifier to treat primary pulmonary hypertension, *Expert Rev. Cardiovasc. Ther.* 3 (2005) 565–569.
- [22] V. Sethi, H. Onyuksel, I. Rubinstein, Liposomal vasoactive intestinal peptide, *Meth. Enzymol.* 391 (2005) 377–395.
- [23] F. Hajos, B. Stark, S. Hensler, R. Prassl, W. Mosgoeller, Inhalable liposomal formulation for vasoactive intestinal peptide, *Int. J. Pharm.* 357 (2008) 286–294.
- [24] H. Inooka, T. Ohtaki, O. Kitahara, T. Ikegami, S. Endo, C. Kitada, K. Ogi, H. Onda, M. Fujino, M. Shirakawa, Conformation of a peptide ligand bound to its G-protein coupled receptor, *Nat. Struct. Biol.* 8 (2001) 161–165.
- [25] C. Sun, D. Song, R.A. Davis-Taber, L.W. Barrett, V.E. Scott, P.L. Richardson, A. Pereda-Lopez, M.E. Uchic, L.R. Solomon, M.R. Lake, K.A. Walter, P.J. Hajduk, E.T. Olejniczak, Solution structure and mutational analysis of pituitary adenylate cyclase-activating polypeptide binding to the extracellular domain of PAC1-RS, *Proc. Natl. Acad. Sci. U.S.A.* 104 (2007) 7875–7880.
- [26] C.R. Grace, M.H. Perrin, J. Gulyas, M.R. Digruccio, J.P. Cantle, J.E. Rivier, W.W. Vale, R. Riek, Structure of the N-terminal domain of a type B1 G protein-coupled receptor in complex with a peptide ligand, *Proc. Natl. Acad. Sci. U.S.A.* 104 (2007) 4858–4863.
- [27] S. Runge, H. Thogersen, K. Madsen, J. Lau, R. Rudolph, Crystal structure of the ligand-bound glucagon-like peptide-1 receptor extracellular domain, *J. Biol. Chem.* 283 (2008) 11340–11347.
- [28] C. Parthier, M. Kleinschmidt, P. Neumann, R. Rudolph, S. Manhart, D. Schlenzig, J. Fanghanel, J.U. Rahfeld, H.U. Demuth, M.T. Stubbs, Crystal structure of the incretin-bound extracellular domain of a G protein-coupled receptor, *Proc. Natl. Acad. Sci. U.S.A.* 104 (2007) 13942–13947.
- [29] A.A. Pioszak, H.E. Xu, Molecular recognition of parathyroid hormone by its G protein-coupled receptor, *Proc. Natl. Acad. Sci. U.S.A.* 105 (2008) 5034–5039.
- [30] G. Gololobov, Y. Noda, S. Sherman, I. Rubinstein, J. Baranowska-Kortylewicz, S. Paul, Stabilization of vasoactive intestinal peptide by lipids, *J. Pharmacol. Exp. Ther.* 285 (1998) 753–758.
- [31] Y.V. Tan, A. Couvineau, S. Murail, E. Ceraudo, J.M. Neumann, J.J. Lacapere, M. Laburthe, Peptide agonist docking in the N-terminal ectodomain of a class II G protein-coupled receptor, the VPAC1 receptor. Photoaffinity, NMR, and molecular modeling, *J. Biol. Chem.* 281 (2006) 12792–12798.
- [32] T. Tenno, N. Goda, Y. Tateishi, H. Tochio, M. Mishima, H. Hayashi, M. Shirakawa, H. Hiroaki, High-throughput construction method for expression vector of peptides for NMR study suited for isotopic labeling, *Protein Eng. Des. Sel.* 17 (2004) 305–314.
- [33] D. Neri, T. Szyperki, G. Otting, H. Senn, K. Wuthrich, Stereospecific nuclear magnetic resonance assignments of the methyl groups of valine and leucine in the DNA-binding domain of the 434 repressor by biosynthetically directed fractional <sup>13</sup>C labeling, *Biochemistry* 28 (1989) 7510–7516.

- [34] L.E. Kay, P. Keifer, T. Saarinen, Pure absorption gradient enhanced heteronuclear single quantum correlation spectroscopy with improved sensitivity, *J. Am. Chem. Soc.* 114 (1992) 10663–10665.
- [35] F. Delaglio, S. Grzesiek, G.W. Vuister, G. Zhu, J. Pfeifer, A. Bax, NMRPipe: a multidimensional spectral processing system based on UNIX pipes, *J. Biomol. NMR* 6 (1995) 277–293.
- [36] T. Herrmann, P. Guntert, K. Wuthrich, Protein NMR structure determination with automated NOE assignment using the new software CANDID and the torsion angle dynamics algorithm DYANA, *J. Mol. Biol.* 319 (2002) 209–227.
- [37] P. Guntert, Automated NMR protein structure calculation, *Prog. Nucl. Magn. Reson. Spectrosc.* 43 (2003) 105–125.
- [38] T. D. Goddard, D. G. Kneller, Sparky 3. San Francisco: University of California.
- [39] G. Cornilescu, F. Delaglio, A. Bax, Protein backbone angle restraints from searching a database for chemical shift and sequence homology, *J. Biomol. NMR* 13 (1999) 289–302.
- [40] J. Fahrenkrug, B. Ottesen, C. Palle, Non-amidated forms of VIP (glycine-extended VIP and VIP-free acid) have full bioactivity on smooth muscle, *Regul. Pept.* 26 (1989) 235–239.
- [41] J. Cavanagh, W.J. Fairbrother III, A.G. Palmer, M. Rance, N.J. Skelton, *Protein NMR Spectroscopy: Principles and Practice*, 2nd Ed, Academic Press, San Diego, 2007, pp. 535–673.
- [42] F. Chevalier, J. Lopez-Prados, P. Groves, S. Perez, M. Martin-Lomas, P.M. Nieto, Structure and dynamics of the conserved protein GPI anchor core inserted into detergent micelles, *Glycobiology* 16 (2006) 969–980.
- [43] P. Nicole, L. Lins, C. Rouyer-Fessard, C. Drouot, P. Fulcrand, A. Thomas, A. Couvineau, J. Martinez, R. Brasseur, M. Laburthe, Identification of key residues for interaction of vasoactive intestinal peptide with human VPAC1 and VPAC2 receptors and development of a highly selective VPAC1 receptor agonist. Alanine scanning and molecular modeling of the peptide, *J. Biol. Chem.* 275 (2000) 24003–24012.
- [44] N. Komi, K. Okawa, Y. Tateishi, M. Shirakawa, T. Fujiwara, H. Akutsu, Structural analysis of pituitary adenylate cyclase-activating polypeptides bound to phospholipid membranes by magic angle spinning solid-state NMR, *Biochim. Biophys. Acta* 1768 (2007) 3001–3011.
- [45] S.R.J. Hoare, Mechanisms of peptide and nonpeptide ligand binding to Class B G-protein-coupled receptors, *Drug Discov. Today* 10 (2005) 417–427.
- [46] M. O'Donnell, R.J. Garippa, N.C. O'Neill, D.R. Bolin, J.M. Cottrell, Structure-activity studies of vasoactive intestinal polypeptide, *J. Biol. Chem.* 266 (1991) 6389–6392.
- [47] H. Igarashi, T. Ito, W. Hou, S.A. Mantey, T.K. Pradhan, C.D. Ulrich, S.J. Hocart, D.H. Coy, R.T. Jensen, Elucidation of vasoactive intestinal peptide pharmacophore for VPAC(1) receptors in human, rat, and guinea pig, *J. Pharmacol. Exp. Ther.* 301 (2002) 37–50.
- [48] H. Igarashi, T. Ito, S.A. Mantey, T.K. Pradhan, W. Hou, D.H. Coy, R.T. Jensen, Development of simplified vasoactive intestinal peptide analogs with receptor selectivity and stability for human vasoactive intestinal peptide/pituitary adenylate cyclase-activating polypeptide receptors, *J. Pharmacol. Exp. Ther.* 315 (2005) 370–381.
- [49] E. Ceraudo, S. Murail, Y.V. Tan, J.J. Lacapere, J.M. Neumann, A. Couvineau, M. Laburthe, The vasoactive intestinal peptide (VIP) alpha-helix up to C terminus interacts with the N-terminal ectodomain of the human VIP/Pituitary adenylate cyclase-activating peptide 1 receptor: photoaffinity, molecular modeling, and dynamics, *Mol. Endocrinol.* 22 (2008) 147–155.



# *$^1\text{H}$ , $^{13}\text{C}$ , and $^{15}\text{N}$ resonance assignment of the first PDZ domain of mouse ZO-1*

*Yoshitaka Umetsu, Natsuko Goda, Ryo Taniguchi, Kaori Satomura, Takahisa Ikegami, Mikio Furuse & Hidekazu Hiroaki*

**Biomolecular NMR Assignments**

ISSN 1874-2718

Volume 5

Number 2

Biomol NMR Assign (2011)

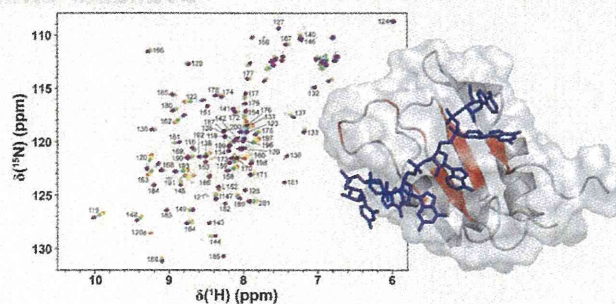
5:207-210


DOI 10.1007/s12104-011-9301-x

Volume 5 Number 2 2009 ISSN 1874-2718

## **Biomolecular NMR Assignments**

editor in chief:  
A.G. Palmer III



 Springer

 Springer



Your article is protected by copyright and all rights are held exclusively by Springer Science+Business Media B.V.. This e-offprint is for personal use only and shall not be self-archived in electronic repositories. If you wish to self-archive your work, please use the accepted author's version for posting to your own website or your institution's repository. You may further deposit the accepted author's version on a funder's repository at a funder's request, provided it is not made publicly available until 12 months after publication.



# $^1\text{H}$ , $^{13}\text{C}$ , and $^{15}\text{N}$ resonance assignment of the first PDZ domain of mouse ZO-1

Yoshitaka Umetsu · Natsuko Goda ·  
Ryo Taniguchi · Kaori Satomura · Takahisa Ikegami ·  
Mikio Furuse · Hidekazu Hiroaki

Received: 7 January 2011 / Accepted: 12 March 2011 / Published online: 24 March 2011  
© Springer Science+Business Media B.V. 2011

**Abstract** Zonula occludens-1 (ZO-1) is a scaffolding molecule critical to the formation of intercellular adhesion structures, such as tight junctions (TJs) and adherens junctions (AJs). ZO-1 contains three PDZ domains followed by a GUK domain and a ZU5 domain. The first PDZ of ZO-1 (ZO-1(PDZ1)) serves as a protein–protein interaction module and interacts with the C-termini of almost all claudins to initiate the formation of a belt-like structure on the lateral membranes, thereby promoting TJ formation. It has been recently reported that approximately 15% of all PDZ domains bind phosphoinositides, and ZO-1(PDZ1) is the one of these. Here we report the  $^{15}\text{N}$ ,  $^{13}\text{C}$ , and  $^1\text{H}$  chemical shift assignments of the first PDZ domain of mouse ZO-1. The resonance assignments obtained in this work may contribute in clarifying the interplay between the two binary interactions, ZO-1(PDZ1)–claudins and ZO-1(PDZ1)–phospholipids, and suggesting a novel regulation mechanism

underlying the formation and maintenance of cell–cell adhesion machinery downstream of the phospholipid signaling pathways.

**Keywords** Cell–cell adhesion · Tight junction · ZO-1; PDZ domain · Phosphoinositide

## Biological context

The tight junction (TJ), or zonula occludens, is the most apical intercellular junctional complex found in epithelial and endothelial cells. It is believed that TJs maintain the major epithelial and endothelial barrier functions, thus maintaining the unique composition of chemical and biological substances at the apical and basolateral spaces of the cell layer (Furuse et al. 1993; Ikenouchi et al. 2007). TJs are responsible for the formation of barriers regulating the passage of solutes and cells through the paracellular space. In addition to their semipermeable barrier and/or gate function, TJs are also involved in some signal transduction pathways, i.e., they regulate their own assembly and barrier function, as well as transmit signals from the paracellular space to the cell interior by coordinating a variety of signaling and trafficking molecules that regulate cell differentiation, proliferation, and polarity (Tsukita et al., 2001; Ikenouchi et al. 2005; Martin-Padura et al. 1998).

The extracellular part of TJs is composed of four families of integral membrane proteins, claudins (Furuse et al. 1998; Morita et al. 2003), occludin (Furuse et al. 1993), junctional adhesion molecules (JAMs) (Martin-Padura et al. 1998), and tricellulin (Ikenouchi et al. 2005). Most of these membrane proteins are linked to each other by PDZ (PSD95/Discs large/ZO-1) domain-containing scaffold proteins. The PDZ

Y. Umetsu · N. Goda · R. Taniguchi · K. Satomura · H. Hiroaki  
Division of Structural Biology Graduate School of Medicine,  
Kobe University, Kobe, Hyogo, Japan

K. Satomura · M. Furuse · H. Hiroaki  
Targeted Protein Research Program (JST-TPRP),  
Kobe University, Kobe, Hyogo, Japan

T. Ikegami  
Institute for Protein Research, Osaka University,  
Suita, Osaka, Japan

M. Furuse · H. Hiroaki (✉)  
Global-COE (Center of Excellence) Program for Integrative  
Membrane Biology, Kobe University, Kobe, Hyogo, Japan  
e-mail: hiroakih@med.kobe-u.ac.jp

M. Furuse  
Division of Cell Biology, Graduate School of Medicine,  
Kobe University, Kobe, Hyogo, Japan

domain is compact and globular. It is the most abundant peptide-binding module in the human genome, in which there may be as many as 440 PDZ domains in 259 different proteins (Letunic et al. 2004). In TJs, membrane-associated guanylate kinase (MAGUK) proteins, ZO-1, and ZO-2 are localized exclusively in polarized epithelia (Gonzalez-Mariscal et al. 2000; Gonzalez-Mariscal et al. 2003).

Here we describe the NMR assignments of the first PDZ domain of ZO-1, ZO-1(PDZ1). As well as most other PDZ domain-containing proteins, ZO-1 and ZO-2 are multiple tandem PDZ domains that harbor other protein-binding modules, such as SH3 and ZU5 domains, thereby functioning as a scaffold. One of the pivotal interactions in junctional complexes is that between the first PDZ domains from ZO-1 or ZO-2 and the cytosolic C-terminal PDZ-binding motif of claudins (Itoh et al. 1999). More recently, approximately 15% of PDZ domains were shown to interact with phospholipids directly (Wu et al. 2007; Zimmermann 2006), and ZO-1(PDZ1) and ZO-1(PDZ2) are examples in the case (Meerschaert et al. 2009). Thus, the resonance assignments of ZO-1(PDZ1) contribute to the study of the interactions between ZO-1(PDZ1) and claudins or other ligands, such as phosphoinositides.

## Methods and experiments

### Sample preparation

The expression vector for the recombinant GST-tagged form of mouse ZO-1(PDZ1) (residues 18–110) was constructed using PRESAT-vector methodology (Tenno et al. 2004). Isotopically labeled protein for NMR spectroscopy was generated in *Escherichia coli* BL21(DE3) from 1 L M9 minimal medium culture grown at 20°C in the presence of [<sup>15</sup>N]-NH<sub>4</sub>Cl and [<sup>13</sup>C]-glucose as the sole nitrogen and carbon sources, respectively. The harvested cells were resuspended in lysis buffer (50 mM Tris-HCl, pH 7.5, 150 mM NaCl) and disrupted by sonication. The supernatant was applied to a DEAE-Sepharose (GE Healthcare) column and then affinity purified by Glutathione Sepharose 4 Fast Flow (GE Healthcare) chromatography. The GST tag was removed by PreScission protease on beads. Next, the ZO-1(PDZ1) was purified by gel filtration using a HiLoad 26/60 Superdex 75 pg (GE Healthcare). Using this purification protocol, <sup>15</sup>N-labeled or <sup>13</sup>C, <sup>15</sup>N-doubly-labeled ZO-1(PDZ1) was prepared. The purified protein was concentrated to 0.73 mM and dialyzed with 22 mM MES (pH 5.9). The protein solution (313.5 μL) and 16.5 μL 99% D<sub>2</sub>O were mixed, resulting in 0.7 mM ZO-1(PDZ1) in 20 mM MES (pH 5.9) in 95% H<sub>2</sub>O–5% D<sub>2</sub>O. <sup>14</sup>N-amino-acid-selective-inversely-labeled <sup>15</sup>N-labeled-ZO-1(PDZ1) was also prepared. (Arg<sup>-</sup>)- and (Lys<sup>-</sup>)-<sup>15</sup>N-labeled-ZO-1(PDZ1) were

prepared from 0.5 L <sup>15</sup>N-enriched M9 media supplemented with <sup>14</sup>N-Lys or <sup>14</sup>N-Arg, respectively. (The details of the protocol are in preparation.)

### NMR spectroscopy

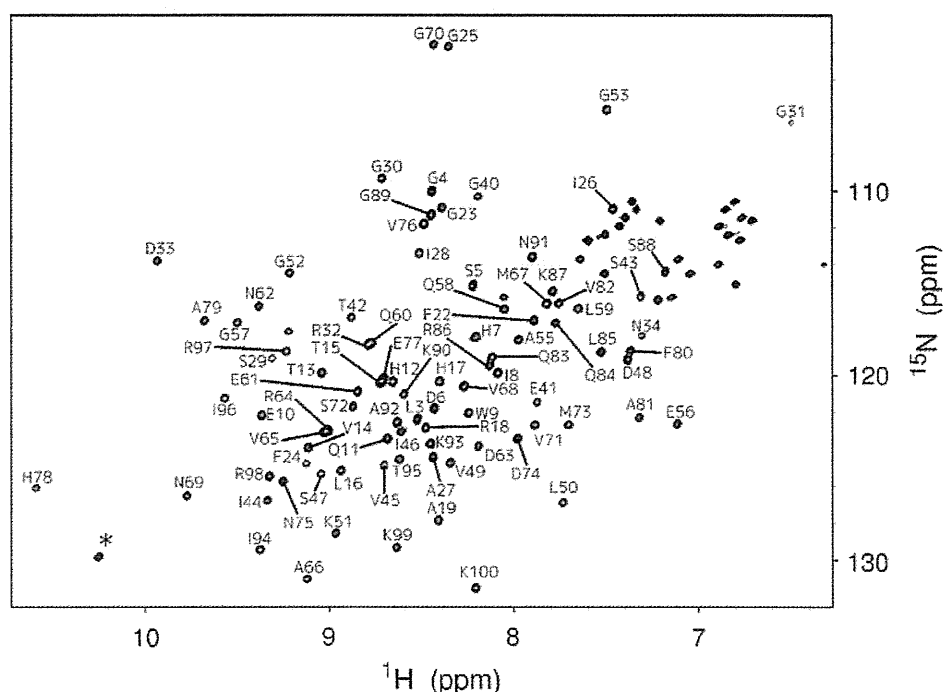
NMR experiments were performed on a Bruker AvanceDRX (600 MHz) or an Avance III (600 MHz) NMR spectrometer (Bruker), the latter was equipped with a cryogenic triple-resonance probe. For the assignment of backbone <sup>1</sup>H, <sup>13</sup>C, and <sup>15</sup>N resonances, HNCA, HN(CO)CA, HNCACB, CBCA(CO)NH, HNC(O), HN(CA)CO, and 3D <sup>15</sup>N-edited-NOESY-HSQC spectra were recorded. For side chain resonance assignment, 2D constant-time <sup>1</sup>H-<sup>13</sup>C HSQC, 3D <sup>13</sup>C-edited-NOESY-HSQC, HCCH-TOCSY, CC(CO)NNH, and HCC(CO)NNH spectra were recorded. All NMR spectra were recorded at 298 K. All spectra were processed using NMRPipe (Delaglio et al. 1995) and analyzed using the program SPARKY (Goddard and Kneller 2004).

### Assignments and data deposition

The sequential assignment of backbone signals was initiated by the automatic program MARS (Jung and Zweckstetter 2004), resulting in approximately 60% completion. However, subsequent iterative MARS runs could not increase further assignment gains beyond 65%. We then carefully traced the sequential connectivities based on triple-resonance data sets. Further help with assignment was provided by the <sup>15</sup>N-edited NOESY spectra. These backbone assignments were confirmed by a visual inspection of <sup>15</sup>N-HSQC spectra of (Lys<sup>-</sup>)-(Arg<sup>-</sup>)-inversely labeled ZO-1(PDZ1).

Following a sequential assignment procedure, 94.7% of the <sup>1</sup>H<sup>N</sup>, <sup>15</sup>N resonances of the backbone amide groups (90 out of the 95 non-Pro residues) were assigned (Fig. 1). In addition, 93.0% of H<sup>α</sup> (93 out of 100 residues), 94.0% of <sup>13</sup>C<sup>α</sup> (94 out of 100 residues), and 94.3% of <sup>13</sup>C<sup>β</sup> (82 out of 87 residues) resonances were assigned. The secondary structure of ZO-1(PDZ-1) was predicted by comparing the chemical shifts with random coil values using TALOS program. This result and our preliminary structural analysis of ZO-1(PDZ-1) indicate six β-strands (Glu10-Leu16, Ile26-Ser29, Val45-Val49, Arg64-Val68, Val71-Ser72, and Ala92-Arg98) and an α-helix (Glu77-Lys87), in good agreement with the structural elements of crystal structure of ZO-1(PDZ-1) (PDB: 2H3 M) (Appleton et al. 2006). The sequential correlations of the backbone resonances of His36, Phe37, Gln38, and Ser39 were missing. On the <sup>1</sup>H-<sup>15</sup>N HSQC spectra, there was only one unassigned main-chain amide proton resonance, which may correspond to one of these residues. The residues are involved in the long loop

**Fig. 1** A portion of the  $^{15}\text{N}$ - $^1\text{H}$ -HSQC spectrum of the first PDZ domain of mouse ZO-1 protein illustrating a number of the assigned backbone  $^{15}\text{N}$  resonances. Asterisk indicates the Trp9 side chain



between  $\beta 2$  and  $\beta 3$ . In the crystal structure of ZO-1(PDZ1), the loop adopted a compact L-like structure and was closed toward the  $\beta 2$  surface. However, part of the loop had some contact with the neighboring molecule in the crystal lattice, suggesting that this folded structure may not be natural in solution. In our preliminary analysis of the solution structure of ZO-1(PDZ1), this folded loop structure was not observed (manuscript in preparation). It is likely that the loop, including the four “missing residues,” adopts a loose, extended conformation in certain structural equilibrium.

Because of the sample preparation from the GST-fusion protein construct, the NMR sample must contain the extra seven residues (GPLGSDH) preceding the N-terminus in mouse ZO-1 (residues 18–110) in the sample. Thus, in the chemical shift data and Fig. 1, the residues 1–7 correspond to GPLGSDH from the expression vector, whereas the residues 8–100 are equivalent to the residues 18–110 of the full length mouse ZO-1. The assigned chemical shifts of ZO-1(PDZ1) have been deposited in the BioMagResBank under accession number 11424.

**Acknowledgments** This work was supported by a Grant-in-Aid from Bioinformatics Research and Development (BIRD) and Target Protein Research Program (TPRP) of the Japan Scientific and Technology Cooperation (JST).

## References

- Appleton BA, Zhang Y, Wu P, Yin JP, Hunziker W, Skelton NJ, Sidhu SS, Wiesmann C (2006) Comparative structural analysis of the Erbin PDZ domain and the first PDZ domain of ZO-1. Insights into determinants of PDZ domain specificity. *J Biol Chem* 281:22312–22320
- Delaglio F, Grzesiek S, Vuister GW, Zhu G, Pfeifer J, Bax A (1995) NMRPipe: a multidimensional spectral processing system based on UNIX pipes. *J Biomol NMR* 6:277–293
- Furuse M, Hirase T, Itoh M, Nagafuchi A, Yonemura S, Tsukita S, Tsukita S (1993) Occludin: a novel integral membrane protein localizing at tight junctions. *J Cell Biol* 123:1777–1788
- Furuse M, Fujita K, Hiiiragi T, Fujimoto K, Tsukita S (1998) Claudin-1 and -2: novel integral membrane proteins localizing at tight junctions with no sequence similarity to occludin. *J Cell Biol* 141:1539–1550
- Goddard TD, Kneller DG (2004) Sparky 3. University of California, San Francisco
- Gonzalez-Mariscal L, Betanzos A, Avila-Flores A (2000) MAGUK proteins: structure and role in the tight junction. *Semin Cell Dev Biol* 11:315–324
- Gonzalez-Mariscal L, Betanzos A, Nava P, Jaramillo BE (2003) Tight junction proteins. *Prog Biophys Mol Biol* 81:1–44
- Ikenouchi J, Furuse M, Furuse K, Sasaki H, Tsukita S, Tsukita S (2005) Tricellulin constitutes a novel barrier at tricellular contacts of epithelial cells. *J Cell Biol* 171:939–945
- Ikenouchi J, Umeda K, Tsukita S, Furuse M, Tsukita S (2007) Requirement of ZO-1 for the formation of belt-like adherens junctions during epithelial cell polarization. *J Cell Biol* 176:779–786
- Itoh M, Furuse M, Morita K, Kubota K, Saitou M, Tsukita S (1999) Direct binding of three tight junction-associated MAGUKs, ZO-1, ZO-2, and ZO-3, with the COOH termini of claudins. *J Cell Biol* 147:1351–1363
- Jung YS, Zweckstetter M (2004) Mars—robust automatic backbone assignment of proteins. *J Biomol NMR* 30:11–23
- Letunic I, Copley RR, Schmidt S, Ciccarelli FD, Doerks T, Schultz J, Ponting CP, Bork P (2004) SMART 4.0: towards genomic data integration. *Nucleic Acids Res* 32(Database issue):142–144
- Martin-Padura I, Lostaglio S, Schneemann M, Williams L, Romano M, Fruscella P, Panzeri C, Stoppacciaro A, Ruco L, Villa A,

- Simmons D, Dejana E (1998) Junctional adhesion molecule, a novel member of the immunoglobulin superfamily that distributes at intercellular junctions and modulates monocyte transmigration. *J Cell Biol* 142:117–127
- Meerschaert K, Tun MP, Remue E, De Ganck A, Boucherie C, Vanloo B, Degeest G, Vandekerckhove J, Zimmermann P, Bhardwaj N, Lu H, Cho W, Gettemans J (2009) The PDZ2 domain of zonula occludens-1 and -2 is a phosphoinositide binding domain. *Cell Mol Life Sci* 66:3951–3966
- Morita K, Sasaki H, Furuse K, Furuse M, Tsukita S, Miyachi Y (2003) Expression of claudin-5 in dermal vascular endothelia. *Exp Dermatol* 12:289–295
- Tenno T, Goda N, Tateishi Y, Tochio H, Mishima M, Hayashi H, Shirakawa M, Hiroaki H (2004) High-throughput construction method of expression vector of peptides for NMR study suited for isotopic labeling. *Protein Eng. Des. Sel.* 17:305–314
- Tsukita S, Furuse M, Itoh M (2001) Multifunctional strands in tight junctions. *Nat Rev Mol Cell Biol* 2:285–293
- Wu H, Feng W, Chen J, Chan LN, Huang S, Zhang M (2007) PDZ domains of Par-3 as potential phosphoinositide signaling integrators. *Mol Cell* 28:886–898
- Zimmermann P (2006) The prevalence and significance of PDZ domain-phosphoinositide interactions. *Biochim Biophys Acta* 1761:947–956